

# Source apportionment of wide range particle size spectra and black carbon collected at the airport of Venice (Italy)

Masiol, Mauro; Vu, Tuan V.; Beddows, David; Harrison, Roy

DOI:

[10.1016/j.atmosenv.2016.05.018](https://doi.org/10.1016/j.atmosenv.2016.05.018)

License:

Creative Commons: Attribution-NonCommercial-NoDerivs (CC BY-NC-ND)

*Document Version*

Peer reviewed version

*Citation for published version (Harvard):*

Masiol, M, Vu, TV, Beddows, D & Harrison, R 2016, 'Source apportionment of wide range particle size spectra and black carbon collected at the airport of Venice (Italy)', *Atmospheric Environment*, vol. 139, pp. 56-74.  
<https://doi.org/10.1016/j.atmosenv.2016.05.018>

[Link to publication on Research at Birmingham portal](#)

## **Publisher Rights Statement:**

Checked May 2016

## **General rights**

Unless a licence is specified above, all rights (including copyright and moral rights) in this document are retained by the authors and/or the copyright holders. The express permission of the copyright holder must be obtained for any use of this material other than for purposes permitted by law.

- Users may freely distribute the URL that is used to identify this publication.
- Users may download and/or print one copy of the publication from the University of Birmingham research portal for the purpose of private study or non-commercial research.
- User may use extracts from the document in line with the concept of 'fair dealing' under the Copyright, Designs and Patents Act 1988 (?)
- Users may not further distribute the material nor use it for the purposes of commercial gain.

Where a licence is displayed above, please note the terms and conditions of the licence govern your use of this document.

When citing, please reference the published version.

## **Take down policy**

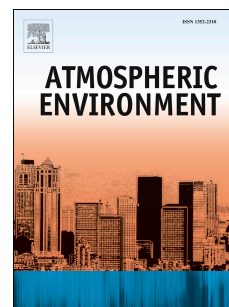
While the University of Birmingham exercises care and attention in making items available there are rare occasions when an item has been uploaded in error or has been deemed to be commercially or otherwise sensitive.

If you believe that this is the case for this document, please contact [UBIRA@lists.bham.ac.uk](mailto:UBIRA@lists.bham.ac.uk) providing details and we will remove access to the work immediately and investigate.

# Accepted Manuscript

Source apportionment of wide range particle size spectra and black carbon collected at the airport of Venice (Italy)

Mauro Masiol, Tuan V. Vu, David C.S. Beddows, Roy M. Harrison



PII: S1352-2310(16)30359-4

DOI: [10.1016/j.atmosenv.2016.05.018](https://doi.org/10.1016/j.atmosenv.2016.05.018)

Reference: AEA 14606

To appear in: *Atmospheric Environment*

Received Date: 18 November 2015

Revised Date: 6 May 2016

Accepted Date: 9 May 2016

Please cite this article as: Masiol, M., Vu, T.V., Beddows, D.C.S., Harrison, R.M., Source apportionment of wide range particle size spectra and black carbon collected at the airport of Venice (Italy), *Atmospheric Environment* (2016), doi: 10.1016/j.atmosenv.2016.05.018.

This is a PDF file of an unedited manuscript that has been accepted for publication. As a service to our customers we are providing this early version of the manuscript. The manuscript will undergo copyediting, typesetting, and review of the resulting proof before it is published in its final form. Please note that during the production process errors may be discovered which could affect the content, and all legal disclaimers that apply to the journal pertain.

**SOURCE APPORTIONMENT OF WIDE  
RANGE PARTICLE SIZE SPECTRA AND  
BLACK CARBON COLLECTED AT THE  
AIRPORT OF VENICE (ITALY)**

**Mauro Masiol, Tuan V. Vu, David C.S. Beddows and  
Roy M. Harrison<sup>\*†</sup>**

**Division of Environmental Health and Risk Management  
School of Geography, Earth and Environmental Sciences  
University of Birmingham  
Edgbaston, Birmingham B15 2TT  
United Kingdom**

---

<sup>\*</sup> To whom correspondence should be addressed.

Tele: +44 121 414 3494; Fax: +44 121 414 3708; Email: r.m.harrison@bham.ac.uk

<sup>†</sup>Also at: Department of Environmental Sciences / Center of Excellence in Environmental Studies, King Abdulaziz University, PO Box 80203, Jeddah, 21589, Saudi Arabia

**HIGHLIGHTS**

- Particle number, size and black carbon were measured at the airport of Venice
- Data were analysed along with gases, weather parameters and flight traffic
- Six potential sources were identified and apportioned by PMF analysis on PNSD
- Airport emissions contributed ~20% to the total PNC
- No specific local sources of BC can be identified as dominant

**ABSTRACT**

Atmospheric particles are of high concern due to their toxic properties and effects on climate, and large airports are known as significant sources of particles. This study investigates the contribution of the Airport of Venice (Italy) to black carbon (BC), total particle number concentrations (PNC) and particle number size distributions (PNSD) over a large range (14 nm to 20  $\mu$ m). Continuous measurements were conducted between April and June 2014 at a site located 110 m from the main taxiway and 300 m from the runway. Results revealed no significantly elevated levels of BC and PNC, but exhibited characteristic diurnal profiles. PNSD were then analyzed using both *k*-means cluster analysis and positive matrix factorization. Five clusters were extracted and identified as midday nucleation events, road traffic, aircraft, airport and nighttime pollution. Six factors were apportioned and identified as probable sources according to the size profiles, directional association, diurnal variation, road and airport traffic volumes and their relationships to micrometeorology and common air pollutants. Photochemical nucleation accounted for ~44% of total number, followed by road+shipping traffic (26%). Airport-related emissions accounted for ~20% of total PNC and showed a main mode at 80 nm and a second mode beyond the lower limit of the SMPS (<14 nm). The remaining factors accounted for less than 10% of number counts, but were relevant for total volume concentrations: nighttime nitrate, regional pollution and local resuspension. An analysis of BC levels over different wind sectors revealed no especially significant contributions from specific directions associated with the main local sources, but a potentially significant role of diurnal dynamics of the mixing layer on BC levels. The approaches adopted in this study have identified and apportioned the main sources of particles and BC at an international airport located in area affected by a complex emission scenario. The results may underpin measures for improving local and regional air quality, and health impact assessment studies.

**Keywords:** Airport; black carbon; size distributions; source apportionment; ultrafine particles

## 1. INTRODUCTION

Ambient air pollution, particularly airborne particulate matter (PM), exerts a large influence on public opinion and with policy-makers and the scientific community because of its known adverse effects on human health (Heal et al., 2012; Beelen et al., 2014) and its complex implications for climate (Kulmala et al., 2011; Fiore et al., 2012). The transformation and combustion of fossil fuels are amongst the main sources worldwide impacting upon PM and are studied widely because of the increasing demand for energy driven by industrialised countries and the economic growth of emerging regions. Besides the well-recognised sources which combust fossil fuels (e.g., road traffic, shipping, industries, domestic heating), aviation deserves particular attention because of the rapid growth of civil aviation. Despite the occurrence of events of global impact, such as the terrorist attack of 11th September 2001, the outbreak of severe acute respiratory syndrome in 2002–2003 and the recent global economic crisis (2008–2009), civil aviation has experienced an almost constant growth from the 1930s to present day. This trend (about +5% every year) is expected to continue over the next decades (Lee et al., 2009).

The global-scale impacts of civil aviation are heavily debated and are principally attributed to the climate forcing of exhausts emitted at cruising altitudes. In the lower troposphere, civil aviation has more local effects, which are mainly attributed to the noise and the deterioration of air quality at ground-level due to airport operations. Up to today, many studies have been reported on aircraft engine exhaust emissions (Masiol and Harrison, 2014 and references therein), and emission standards for new types of aircraft engine have been implemented since the late 1970s for carbon monoxide (CO), nitrogen oxides ( $\text{NO}_x = \text{NO} + \text{NO}_2$ ), unburned hydrocarbons and smoke number (ICAO, 2008).

However, beside aircraft engine exhausts, other sources may affect air quality around airports, e.g. non-exhaust emissions from aircraft, emissions from the units providing power to the aircraft on the ground, the traffic due to the airport ground service, maintenance work, heating facilities, fugitive vapours from refuelling, transportation systems and road traffic for moving people and goods in and out of the airport. Beyond this complex emission scenario, most large airports are also located near heavily populated urban areas and are responsible for the build-up of some pollutants and exceedence of some air quality standards.

The Marie Skłodowska-Curie project CHEERS (Chemical and Physical Properties and Source Apportionment of Airport Emissions in the context of European Air Quality Directives) was motivated by the lack of information regarding the impacts of airports located near large cities. In particular, the role of airport emissions on the black carbon (BC), particle number concentration (PNC) and particle number size distributions (PNSD) are still debated, although some previous studies have provided evidence that aircraft are major sources of such pollutants. For example, Dodson et al. (2009) found that aircraft activity in close proximity to a small regional airport contributed 24–28% of the total BC measured at five sites 0.16–3.7 km from the airfield; Hudda et al. (2014) concluded that emissions from the Los Angeles international airport increase PNC 4-fold at 10 km downwind; Keuken et al. (2015) reported that the PNSD in an area affected by emissions from Schiphol airport (The Netherlands) was dominated by ultrafine (10 to 20 nm) particles.

This study aims to investigate the impacts of on-airport emissions on the levels of BC, PNC and PNSD over a very wide range (14 nm to 20  $\mu$ m) at a runway/taxiway-side site of the Marco Polo international airport (VCE). The airport is located ~5.5 km N to the historic city centre of Venice and ~6 km NE to the large urban area of Mestre (~270,000 inhabitants). This is an area characterised by many strong local anthropogenic pressures and a Mediterranean climate.

Among the well-established source apportionment methods, cluster analysis and receptor modelling techniques have been widely applied for characterising the PNSD and the most probable sources of airborne particles (e.g., Dall'Osto et al., 2012). Among the cluster analyses, *k*-means is the most widely used technique. Salimi et al. (2014) tested various clustering methods on PNSD data and reported that *k*-means resulted in a highest performance among others. Many studies have successfully applied *k*-means clustering for purposes similar to this study and under weather conditions comparable to N Italy: for example, Wegner et al. (2012) studied the characteristic size distributions in urban background environments; Brines et al. (2014; 2015) categorized PNSD measured in high-insolation cities (Barcelona, Madrid, Rome, Brisbane and Los Angeles), i.e. under weather conditions comparable to Venice; Beddows et al. (2014) explored the variations in tropospheric submicron particle size distributions all across Europe.

Among the receptor modelling techniques, positive matrix factorization (PMF) has been applied to PNSD data: Friend et al. (2013) compared the application of PMF and absolute principal component scores (PCA-APCS) for resolving sources of PNSD along a traffic corridor and concluded that PMF results were more reliable; Ogulei et al. (2007) modelled the source contributions to submicron PNSD measured in Rochester, NY, USA; Harrison et al. (2011) used PMF to quantify the sources of wide size spectra PNSD in the vicinity of a highway.

In this study, particle spectra were used as input for a *k*-means cluster analysis and a PMF receptor model aiming to characterise the PNSD and identify and quantify the main potential sources of particles, respectively. Data were also analysed jointly with common air pollutants, weather parameters and traffic profiles of airport and road traffic to investigate potential sources and formation mechanisms. Furthermore, an analysis of BC levels associated with different wind sectors allowed extraction of information on sources of soot particles and pointed out the effects of mixing layer dynamics on driving the levels of some pollutants in the study area.



## 2. MATERIALS AND METHODS

### 2.1 Site Description

Amongst other regions, the Po Valley (Northern Italy) represents one of the few remaining hotspots in Europe, where the levels of air pollutants (mainly NO<sub>2</sub>, PM<sub>10</sub> and PM<sub>2.5</sub>) are currently breaching the *target* or *limit* values imposed by European Directives. For this reason, the study of the main PM sources in the Po Valley is fundamental and VCE (Figure 1) represents an interesting case study for a number of reasons:

- it is the third airport of Italy for flight traffic with more than 100,000 annual aircraft movements. The major type of aircraft flying at VCE are short- to medium-range, narrow-body, twin-engine airliners: A320 > A319 > A321 > B737-800 > B717;
- it is located close to a densely populated urban area (Mestre), where the levels of particulate matter pollution do not fully comply with the EC limit and target values (Masiol et al., 2014a);
- it is located in a coastal area and is therefore affected by the atmospheric circulation associated with sea/land breezes during the warm season. This circulation may potentially advect the pollutants emitted at the airport toward the mainland during the daytime;
- being located on the eastern edge of the Po Valley, it is potentially affected by the transport of pollutants at regional or even transboundary scales (e.g., Squizzato and Masiol, 2015);
- the air quality scenario of the area is extremely complex because of the high range of differing potential sources, including: (1) high density residential areas mostly using methane for domestic heating, even though the burning of wood (i.e. logs, briquettes, chips and pellets) is nowadays becoming an increasing alternative; (2) heavily trafficked roads which are highly congested during peak hours with light and heavy duty vehicles using gasoline, diesel and LPG fuels; (3) a motorway and a motorway-link which are a part of the main European routes E55 and E70, with the consequent heavy duty vehicle traffic transporting goods between Italy, Eastern and Central Europe; (4) an extended industrial area (Porto Marghera) hosting a large number of different installations, including thermal power plants burning coal, gas and refuse

derived fuels, a large shipbuilding industry, oil-refinery, municipal solid waste incinerators and many other chemical, metallurgical and glass plants; (5) the artistic glassmaking factories in the Island of Murano, which is made up of small and medium-sized glassworks without significant measures for emission abatement; (6) heavy shipping traffic due to public transport, commercial and cruise terminals (annually, 3600–4000 vessels pass throughout the harbour of Venice accounting for a total tonnage of more than 25 billion kg);

- A preliminary study (Valotto et al., 2014) has indicated a potential influence of airport emissions on  $PM_{10}$  mass concentrations, mainly attributed to tyre wear during landing.

The site was set in an airport apron area at ca. 110 m from the main taxiway and ca. 300 m from the runway. The sampling site location (Figure 1) was the best compromise between stringent safety measures for flights and scientific purposes. Sea breezes occur during daytime approx. from April to October and blow air masses from the Adriatic Sea to the mainland (Figure SI1). Aircraft mostly used the runway 04L (landing and takeoff direction predominantly from SW to NE). During the sampling campaign, ~300 aircraft used the runway 22R (opposite direction to 04L, from NE to SW) out of a total of ~9500 flight movements (~3.2%). Under such circumstances, the site was chosen to catch the aircraft plumes and was set in a place downwind of the latter part of the taxiway and the beginning of the runway, where aircraft run their engines at 100% thrust during take-off or where the wheels hit the ground during landing causing smoke clearly visible to the naked eye. This choice was further supported by a modelling study (Pecorari et al., 2015) reporting that the site is affected by aircraft engine plumes for gaseous pollutants. A more detailed analysis of civil aviation traffic and wind direction is provided in Figure SI2: results indicate that a significant number of both takeoffs and landings occurred when the sampling site is downwind of the runway (winds from ~45°-160°).

## 2.2 Instrumentation Suite

An intensive sampling campaign was carried out from 28th April to 9th June 2014 at the VCE site. The period is representative of typical summer wind regimes (Figure SI1), when air masses prevalently blow from NE at nighttime and from SSE during daytime. Ultrafine particle counts and their size distributions from 14.3 to 673.2 nm were measured at 5 min time resolution using a scanning mobility particle sizer spectrometer (SMPS) comprising a TSI 3080 electrostatic classifier, a TSI 3081 differential mobility analyzer (long DMA), a TSI 3087 X-ray aerosol neutraliser and a TSI 3022A condensation particle counter (CPC) based on *n*-butyl alcohol (Fisher Scientific, ACS) condensation. The range of size spectra were complemented by a TSI aerodynamic particle sizer (APS) 3321 which measures particle diameters within the range 0.5–19.8  $\mu\text{m}$ . BC was continuously measured in PM with aerodynamic diameter  $< 2.5 \mu\text{m}$  ( $\text{PM}_{2.5}$ ) with 5 min resolution using a 7-wavelength aethalometer (Magee Scientific AE31). Instrumental set-up: the SMPS operated at a sheath air to aerosol flow ratio of 10:1 (sheath and sample air flow rates were 3.0 and 0.3  $\text{L min}^{-1}$  respectively, voltage 10-9591 V; density 1.2 g/cc; scan time 120 s, retrace 15 s; number of scan 2) while CPC operated at low flow rate (0.3  $\text{L min}^{-1}$ ). APS flow rate was 5  $\text{L min}^{-1}$ .

Instruments were installed into a plastic/metal case over a stand and air inlets were ca. 2 m height and were composed of conductive materials to avoid particle losses and sampling artefacts. Devices were fully serviced, calibrated by authorised companies and underwent internal cross-calibrations with other similar instruments. Moreover, a periodic check and maintenance of instruments and cleaning of inlets was accomplished throughout the sampling campaign.

Weather data including wind speed and direction, air temperature ( $^{\circ}\text{C}$ ), relative humidity (%RH), rain (mm), solar radiation ( $\text{W m}^{-2}$ ) and levels of some pollutants including  $\text{PM}_{2.5}$ , CO, ozone ( $\text{O}_3$ ), nitrogen oxides and sulphur dioxide ( $\text{SO}_2$ ) were also collected hourly at a nearby site (EZI site, Figure 1), which lies ~400 m from the site. Wind data were also collected at a sampling station

located in the industrial area (EZI5), which is indicative of the atmospheric circulation over the whole study area. Traffic data for both civil and general aviation including the type of aircraft, exact time of taxi-in, taxi-out, take-off and landing, were provided by the airport authorities. The profiles of traffic and urban emissions in the nearby urban area were derived from a previous study (Masiol et al., 2014b) which analysed 13 years of air pollution climate at an urban background site in Mestre.

### 2.3 Data Handling and Chemometric Approaches

Data were analysed using R version 3.1.2 (R Core Team, 2015). Preliminary data handling and clean-up were carried out to check the robustness of the dataset, detect anomalous records and to delete outliers. Data greater than the 99.5th percentile and negative values were removed from all the datasets while samples with unreliable behaviour were completely deleted. Missing bins of SMPS or APS data were replaced by linearly interpolated values from the nearest bins to that sample. Missing data for other variables were linearly interpolated between the nearest values of the time series.

In this study, 5-min resolution SMPS and APS spectra were used as input for clustering and PMF analyses. Size spectra were not merged, but a strategy was applied allowing use of raw data. In this way, unmerged spectra have been used also in previous source apportionment studies (e.g., Zhou et al., 2004; Ogulei et al., 2006). Input data were initially handled by averaging groups of three consecutive bins. This procedure has some advantages: (i) reduces the number of variables processed by the PMF, (ii) minimises the noise of raw SMPS data, which may cause high variability amongst consecutive bins and (iii) limits the number of null values (zeros) which are sometimes recorded in the more coarse bins of the SMPS and APS. This way, a total of 51 bins were used as input for PMF: 34 bins from the SMPS ranging from 14.6 nm to 552.3 nm and 17 bins from the APS (0.5–19.8  $\mu\text{m}$ ). In addition the total variable (total number of particles) was calculated

by summing the concentrations of each size bin adjusted with the appropriate multipliers accounting for channel resolutions of the SMPS and APS.

First, the PNSDs were grouped by applying a *k*-means cluster analysis. Details of the adopted method are provided in Beddows et al. (2009; 2014). Essentially, the methodology aims to group single PNSD spectra (SMPS+APS data, 5 min-resolved observations, in this case) into a number *k* of clusters. The partition of each observation into a cluster is based on the similarity of the PNSD spectra with the cluster centroids (means), i.e. the method is optimised to group similarly-shaped PNSD spectra into the same cluster. This strategy has the advantage to group observations with similar spectra, which are likely to be originated by the same set of emission sources or formation processes. The optimum number of clusters was determined by an optimisation algorithm based on the shape of the spectra (Beddows et al., 2009).

Subsequently, PMF analysis was performed on SMPS and APS data with 5 min resolution using the USEPA PMF 5 model. Details of the PMF model are reported elsewhere (Paatero and Tapper, 1994; Paatero, 1997; USEPA, 2014; Hopke, 2016) and in supplementary material section SI1, while associated methods are well reviewed in Reff et al. (2007), Belis et al. (2014) and Brown et al. (2015). Uncertainty associated with the concentration data have been calculated by following a series of steps. Details are provided in supplementary material section SI2.

A series of R packages including ‘Openair’ (Carslaw and Ropkins, 2012) were additionally used to analyse some raw data, to link pollutant levels and PMF source contributions to the local atmospheric circulation and to detect the most probable local sources through bivariate polar plot analysis. Details of polar plots are given in Carslaw et al. (2006).

### 3. RESULTS AND DISCUSSION

#### 3.1 Overview of Data

The distribution of wind directions and the number of take-offs and landings in relation to the wind directions during the monitoring campaign are provided as supplementary material Figures SI1 and SI2, respectively. The wind roses during the sampling period and those for the warm season are similar, allowing extension of the results of this study to the whole period late spring-early fall.

Results of all collected data are summarised as boxplots in Figure 2a. PNCs were split into 4 ranges: nucleation (14-30 nm), Aitken nuclei (30 to 100 nm), accumulation (0.1 to 1  $\mu\text{m}$ ) and coarse (1 to 19.8  $\mu\text{m}$ ). On average the total PNC was  $\sim 1.4 \cdot 10^4$  particles  $\text{cm}^{-3}$ , of which  $7.3 \cdot 10^3$ ,  $4.3 \cdot 10^3$ ,  $1.4 \cdot 10^3$  and 1.1 particles  $\text{cm}^{-3}$  were classified as nucleation, Aitken, accumulation and coarse ranges, respectively. The total PNC was comparable with particle concentrations normally observed in the Po Valley during summer (Rodríguez et al., 2005; Hamed et al., 2007). The highest average concentrations for other pollutants followed the order (in  $\mu\text{g m}^{-3}$ ): CO (474) > O<sub>3</sub> (76) > NO<sub>x</sub> (53) > NO<sub>2</sub> (47) > PM<sub>2.5</sub> (16) > NO (3.5) > BC (1.2) > SO<sub>2</sub> (0.8).

Figure 2b shows the diurnal profiles of pollutants at local time, flight traffic and weather parameters computed by hourly averaging the data. Nucleation range particles show an evident increase during daytime, which is broadly comparable with the diurnal pattern in solar irradiance. Similar diurnal cycles have been observed in other studies (e.g., Kulmala and Kerminen, 2008; Chen et al., 2011; Hirsikko et al., 2013) and have been attributed to nucleation events driven by photochemical reactions and possibly assisted by turbulent mixing in the atmosphere (Janssen et al., 2012). However, the diurnal cycle of nucleation particles is also very similar to that of air traffic intensity. Aitken, accumulation and coarse particles, CO, nitrogen oxides and BC exhibit highest concentrations in the early morning and secondarily in the evening. These patterns are mainly driven by the interaction of emissions, dispersion and atmospheric chemical processes. Similar

diurnal cycles have been previously observed at an urban background site in Mestre-Venice for gaseous pollutants (Masiol et al., 2014b). Following the complex photochemistry of the NO-NO<sub>2</sub>-O<sub>3</sub> system, the cycle of O<sub>3</sub>, which show a daily peak in the afternoon, is the inverse of the cycle of traffic emissions. Despite the very low concentrations of SO<sub>2</sub> normally recorded over the study area, a daily cycle similar to ozone can be identified. Since the daylight hours of the warm season are characterized by the presence of sea breezes, an influence of the local circulation pattern on the levels of O<sub>3</sub> and SO<sub>2</sub> should be further considered. Figures 2b also shows the daily pattern of wind, showing highest speeds in the afternoon (average 3.5 m s<sup>-1</sup>), which are mainly caused by the influence of sea breezes.

Derived parameters are also show in Figure 2. The NO<sub>2</sub>/NO<sub>x</sub> ratio is indicative of the partitioning of nitrogen oxides. In Europe, despite the efforts to lower the NO<sub>x</sub> emissions, NO<sub>2</sub> levels do not yet meet the targets in many locations, including the study area. This is attributed to a discrepancy between achieving NO<sub>x</sub> emission reductions and NO<sub>2</sub> ambient concentrations (e.g., Grice et al., 2009; Cyrys et al., 2012), which has been related to the growing proportion of diesel-powered vehicles with known high primary (direct) emissions of NO<sub>2</sub> (Carslaw et al., 2007). In the study area (Province of Venice), the emission inventories for 2007/8 (ARPAV, 2014) indicated a cumulative emission of 24.4 Gg NO<sub>x</sub> y<sup>-1</sup>, mainly attributed to road transport (37%), combustion in energy and transformation industries (24%) and other mobile sources and machinery (21%). Airport emissions fall into this latter category: aircraft engines emit NO<sub>x</sub>, and emissions increase with engine thrust, i.e. are higher during take-off and lower in taxi and idle phases. The NO-NO<sub>2</sub> partitioning in the emissions of modern high by-pass turbofan engines is also thrust-dependent: NO<sub>2</sub> is principally emitted at idle, while NO is dominant at higher thrust regimes (Wormhoudt et al., 2007). At a first glance, the diurnal profile of NO<sub>2</sub>/NO<sub>x</sub> ratio can be related to airport emissions due to takeoffs (higher NO), however the daily pattern and value of the ratio are similar to those observed at an urban background site in Mestre-Venice (Masiol et al., 2014b), indicating that vehicular traffic is



probably the most influential source. The level of total oxidants ( $OX=O_3+NO_2$ , in ppbv) is useful to assess the oxidative potential in the atmosphere (Kley et al., 1999). Results show that OX levels are mainly driven by ozone and highest concentrations are recorded in the afternoon.

A preliminary investigation of the location of potential local sources of atmospheric pollutants was assessed by mean of polar plots (Figure 3) and polar annulus (Figure SI3) analysis. Polar plots essentially map the pollutant concentrations by wind speed and direction as a continuous surface (Carslaw and Ropkins, 2012). Polar annuli map the average levels of pollutants by wind direction and hours of the day. Generally, most air pollutants ( $NO$ ,  $NO_2$ ,  $OX$ ,  $SO_2$  and  $PNC$ ) show increasing average concentrations for winds blowing from the SE and SW quadrants,  $CO$  decreases for moderate winds from the South and stronger winds from NW, ozone shows no prevalent sector but increases with wind speed, while  $PM_{2.5}$  and  $BC$  increase in calm wind periods and for moderate/strong winds from E, W and S. In particular, some important insights into the location of potential sources can be extracted from the polar plot analysis:

- $NO$  increases towards the ESE, i.e. from the beginning of the runway, where aircraft generally stop and speed up the engines at full power before takeoff. This finding is also evident if considering the partitioning of  $NO_x$ , which shows a remarkable drop of  $NO_2/NO_x$  toward the runway, indicative of a local source. In addition,  $NO$  also increases toward the S-SW sector probably because of emissions of road traffic in Mestre and shipping in Venice;
- Despite its very low concentration,  $SO_2$  (an excellent tracer for shipping, aircraft and oil refineries) seems to be related more to industrial emissions (SW quadrant) and to the Port of Venice (SE), than to the airport activities (quadrant to NE);
- $PNC$  increases toward the SE and SW quadrants, particularly for strong winds from the South, and to a minor extent, from the NE quadrant. These findings suggest that airport activities are not the main source of particles in the area;



- $PM_{2.5}$  increases towards the East, South and West. Although increases from S and W can be related to external sources such as main roads and urban settlements, the high levels recorded towards the East, which roughly corresponds to the section of runway where planes generally land, may relate to aircraft emissions during landing.

In summary, even though the site was strategically located close to the runway and taxiway, the concurrent effects of multiple emission sources in the study area makes it difficult to assess the contribution made by the airport with simple polar plot analysis on raw data.

Figure 4 shows the median PNSDs calculated over the entire sampling campaign and categorised by time of day (01:00-07:00; 07:00-13:00; 13:00-19:00; 19:00-01:00 local time). Medians, 25th and 75th percentiles for SMPS and APS data were then merged using the algorithm developed by Beddows et al. (2010), which also returns the particle volume concentrations (PVSDs). Results show a significant variation in diurnal modal structures of PNSDs with a main mode ranging from below 14 nm in the daytime periods to ~40-50 nm during nighttime and early morning. There are two main reasons for this results: (i) the increased airport activities (6am-10pm) emitting fresh nucleation particles, as reported by several studies (e.g., Anderson et al., 2005; Kinsey et al., 2010; Mazaheri et al., 2013) and (ii) the potential role of nucleation processes during daytime. In this latter context, the diurnal occurrence of sea breezes cannot be disregarded since it may have a potential role in transporting fresh air masses from the Adriatic Sea and the nearby lagoon, which are affected by large tidal cycles and are known sources of aerosol precursor compounds. The production of secondary ultrafine particles may occur in the marine boundary layer by the nucleation of low vapour pressure gases produced naturally (but also of anthropogenic origin) (e.g., O'Dowd and De Leeuw, 2007; Modini et al., 2009): through (1) homogeneous nucleation and (2) the subsequent particle growth via a number of mechanisms and scavenging of clusters by larger pre-existing particles. However, the diurnal variations may also be linked to the main (primary)

emission sources in the study area, i.e. mobile emissions either from road or maritime sources (commercial and tourist ships, private and public transport boats). On the contrary, PVSDs seem to undergo only modest changes throughout the day, with two main modes at 300-400 nm and 3-5  $\mu\text{m}$ .

### 3.2 *k*-means cluster analysis

Five clusters were extracted by the optimisation algorithm ( $k=5$ ). From a mathematical point of view,  $k=5$  returns optimal parameters (Figure SI4), i.e. a local maximum in the Dunn indices (0.0017) and a silhouette width of 0.43 (Beddows et al., 2009).  $k=5$  is also a good compromise for interpretation of PNSD spectra observations from a practical point of view. Hussein et al. (2014) have reported that is not prudent to describe the PNSD with either too few or too many clusters: few clusters (2–4) are not enough to explain variations and detailed differences in the particle number size distributions observed in the urban atmosphere, while extracting too many ( $> 10$ ) clusters may make the aerosol source attribution more challenging.

The centroids (means) of PNSD clusters are reported as solid lines in Figure 5 along with: (i) their 10th, 25th, 75th and 90th percentile spectra as shaded areas; (ii) the volume size distributions (dashed line); (iii) the hourly counts and (iv) wind roses associated to each cluster. The number of observations in each cluster is reported in Figure SI4. Results show that diurnal count profiles are different for most of the clusters (although cluster 2 and 5 present similar hourly count profiles), while 3 clusters exhibit similar wind roses (cluster 2, 4, 5: winds from SE). To facilitate the interpretation of results, a series of 5 consecutive days (23th May 0:00 to 27th May 23:00) was selected and investigated in depth; the period was chosen to be representative of the typical cycling of clusters and typical meteorological conditions. Figure 6 reports a large number of variables measured within this period, including cluster number counts, airport movements (arrivals+departures), solar radiation, NO, SO<sub>2</sub>, and SMPS data (total PNC for nucleation, Aitken

and accumulation ranges and the contour plot of PNSD). Arrows indicating the wind speed and direction data also accompany the plots to help the interpretation of results.

Cluster 1 accounts for 26% of total clustered observations and presents two distinct peaks: while the finest peak extends beyond the SMPS detection limit (14 nm), the other one is at 25-40 nm. It exhibits a diurnal profile compatible with road traffic, i.e. showing a morning (6-8am) and an evening (5-7pm) rush hour peak and its wind rose shows no dominant wind direction. From Figure 6, it can be noted that observations belonging to cluster 1 may be consecutively dominant for several hours (e.g., 23th May from noon to midnight or 26th May from 6am to 6pm) irrespective of the prevailing wind direction. This finding is compatible with sources present all over the study area. All these insights seem to support its interpretation as traffic-related, i.e. observations with a strong influence of the road traffic emissions.

Cluster 3 accounts for most of observations (29%), mainly measured overnight. Its spectrum presents a single well defined peak at approx. 50 nm and its wind rose exhibits the typical nighttime atmospheric circulation patterns (low NE winds). Figure 6 clearly shows that cluster 3 observations start to rise in number in the late evening (before midnight) and usually drop off to near-zero counts in the early morning (6-8am), while they are rarely recorded in the middle of the day. Consequently, cluster 3 can be interpreted as nighttime pollution, i.e. spectra affected by the rise of atmospheric pollutants due to the reduced height of the mixing layer and, probably, by the formation of nighttime nitrate due to the chemistry driving the heterogeneous reactions of  $\text{N}_2\text{O}_5$  and  $\text{NO}_3$  on aerosol surfaces (Seinfeld and Pandis, 2006; Bertram and Thornton, 2009; Brown and Stutz, 2012).

Cluster 5 (14% of total observations) links spectra peaking at 20 nm and having maximum counts in the afternoon (noon-5pm) with a second minor peak in the morning rush hour (7am). Despite its diurnal profile and wind direction being compatible with the airport emissions, Figure 6 clearly shows that cluster 5 well depicts local nucleation events centred in the early afternoon. Daytime

nucleation events forming particles below 15 nm are often observed in coastal environments and are associated with high  $\cdot\text{OH}$  radical and  $\text{SO}_2$  concentrations, but also with iodine oxide gas-phase processes (O'Dowd et al., 1999; O'Dowd and Hoffmann, 2006). They are also widely observed at southern European sites without a nearby marine influence (Reche et al., 2011). At least 3 nucleation events can be found over the selected period (23th, 24th and 27th May): they can be recognised from their typical “banana” shape (Figure 6). Midday nucleation events start at noon with a huge increment of PNC in the finest nucleation range and, then, particles generally continue to grow over the afternoon, evening and overnight to reach the Aitken and accumulation ranges. Most of the time, cluster 5 observations become dominant for several hours (generally from 4 to 8 h after the event), but the nucleation event generally lasts less than 24 hours.

PNSD spectra and clustering results were further investigated to detect and quantify the number of midday nucleation events during the sampling campaign. Despite the complexity of the emission scenario in VCE, a method similar to Dal Maso et al. (2005) was adopted. Data were visually analysed on a daily basis and midday nucleation events are then identified following well defined criteria: (i) only days with a significant number of non-missing records were evaluated; (ii) nucleation episodes must have a clear boost in particle below 30 nm starting around noon; (iii) most of the spectra in an event must be categorised into the cluster 5; (iv) increases in cluster 5-spectra must prevail over a time span of hours; (v) particles must show signs of growth after an event has been initiated. Following such criteria, 7 events have been successfully recorded from a total of 17 valid days (~40%).

Remaining clusters 2 and 4 both account for 15% of total observations and have similar wind roses (prevailing moderate winds from the E-S sector), which may be compatible with airport emissions. However, they present different PNSD spectra. Cluster 2 links spectra characterised by a particles in the nucleation range and peaking beyond the minimum detection diameter of the SMPS (14 nm),

while cluster 4 groups spectra show a primary mode at 60-100 nm and, secondarily, beyond 14 nm. Most of the literature reports that aircraft engine exhausts emit particles in the nucleation range (Kinsey et al., 2010; Mazaheri et al., 2013; Masiol and Harrison, 2014; Lobo et al., 2012;2015), however, some studies also report a second mode in the accumulation range (e.g., Mazaheri et al., 2009). Looking at the aircraft traffic provided by the airport, it is clear that the hourly counts of cluster 2 well relate with the aircraft movements (Figures 2 and SI2). On the contrary, hourly counts for cluster 4 are pretty constant through the day (Figure 5) and the wind rose also recorded counts for winds blowing from the NNE sector, i.e. toward the airport terminal and aircraft park areas. In this light, it can be hypothesized that cluster 2 represents fresh emissions from taking-off or landing aircraft, whereas, cluster 4 is more related to background levels of particles due to the taxi phases and operations at the gates.

Cluster analysis has helped in identifying the main spectral shapes and their frequency over the sampling period. Results show that the spectra are mainly caused by direct emissions, e.g., road and airport traffic (clusters 1, 2) or atmospheric processes, e.g., mixing layer height and air temperature (cluster 3) and midday nucleation events (cluster 5). However, in an environment with very large anthropogenic influences like VCE, it is likely that spectra can be either influenced by single sources/processes or concurrently shaped by multiple sources. Consequently, PMF analysis may yield the most robust information on the probable sources.

### 3.3 PMF Results

Following the signal-to-noise criterion and known instrumental limits, three variables (12, 14.9 and 18.4  $\mu\text{m}$  size bins) were excluded from the model, while five variables (0.5, 0.6, 0.7, 0.9 and 10  $\mu\text{m}$  particles) were labelled as “weak” by tripling their uncertainties. Two additional variables (15.1 and 16.8 nm) were categorised as weak because of showing high scaled residuals in preliminary runs; the total particle concentration was set as the total variable (weak). A total of 172 samples were

excluded as containing missing or incomplete data. A final matrix composed of 49 variables and 4434 samples was then used as input for the PMF. The model was run several times by investigating solutions between 3 and 10 factors, by changing the extra modelling uncertainty option and by finding the most physically plausible result. Solutions of each preliminary run were investigated to avoid poorly/awfully resolved sources or unstable results by: (i) checking the model diagnostics; (ii) identifying factors having significant inter-factor correlations (Pearson  $r > 0.4$  at  $p < 0.01$ ); (iii) minimising the sums of the squared differences between the scaled residuals for pairs of base runs.

A final 6-factor solution with 9.5% extra uncertainty was selected as the best compromise over the PMF diagnostic results and interpretation reliability for factors. Generally, solutions with less than 6 factors returned many unresolved profiles; 7-factors had higher inter-factor correlations, while for  $> 8$  factors solutions generated profiles with  $Q$  well below the expected (theoretical) value of the residual sum of squares  $Q_{exp}$  and/or no physical meaning. Convergence of the final PMF solution was then ensured over multiple runs for the 6-factor solution using a random starting seed. PMF results were carefully checked by investigating the base model displacement error estimation (DISP) and bootstrapping (BS) error estimation (Paatero et al., 2014; Brown et al., 2015). Diagnostics reported that: (i) no factor swaps occurred for DISP analysis indicating that there are not significant rotational ambiguities and the solution is sufficiently robust to be used; (ii) factor mapping from the BS runs suggested that the BS uncertainties can be interpreted and the selected number of factors is appropriate. PMF rotational ambiguities were further assessed by varying the FPEAK value (Paatero et al. 2002) between -5 and 10 and checking the relative changes in  $Q$ , the total number of negative contributions and the G-space plots for edges. The more physically realistic and independent solutions were obtained for FPEAK = 2.5. Uncertainties of FPEAK-rotated solutions were finally estimated over  $n=200$  BS runs.

The extracted factor profiles are presented in Figure 7 as normalised number and volume fractions, while uncertainties of the final solution are shown in Figure SI5 as percentage of species sum with the associated uncertainty estimated by BS. A summary of PMF results is also provided in Table 1.

A first attempt to link PMF factors with airport traffic was carried out by computing Spearman correlations among factor contributions and real airport traffic movements (total, arrivals, departures) at 5 min resolution. Airport traffic was elaborated to return the more plausible number of aircraft movements every 5 min and takes in account the exact timing of each movement. Traffic data include the timings of landing and parking at the terminal (for arrivals) and the timings of departure from gates and take-off (for departures). This way, each movement was adjusted for the real time that each aircraft was moving. The dataset was also handled to maximise the signal of aircraft, i.e. selecting hours with high airport traffic (10am-9pm) and wind regimes blowing air masses from the taxiway and runway to the sampling site (45 to 170 degree). No one factor showed significant ( $p < 0.001$ ) strong ( $\rho > 0.6$ ) or even weak ( $0.35 < \rho < 0.6$ ) correlation with airport traffic. This result may be explained by a number of reasons: (i) airport emissions are complicated to model and predict due to the large number of different phases in the LTO cycles: even if it possible to know the exact time of each movement, it is difficult to predict the timing and the relative position of aircraft at different phases (e.g., the time spent by aircraft in the queue at the beginning of the runway was not recorded or when they are exactly upwind of the sampling site); (ii) although aircraft engines are expected to be the larger contributors to the air pollution at the airport, other sources may interfere by emitting particles with similar size distributions and, then, adding noise to the PMF results (e.g., the aircraft auxiliary power units (APU), which are small on-board turbines providing a source of electrical power and compressed air when aircraft are parked at the gate and sometimes during taxi); (iii) other strong sources are present in the study area; (iv) wind data are recorded hourly and then interpolated for obtaining 5 min time resolution, therefore unknown



discrepancies may occur between estimated and real wind data. This latter point was overcome by investigating 1 h-averaged traffic and PMF data, but correlations were still low for all of the factors.

Due the inability to link PMF factors directly with aircraft movements, the interpretation of the extracted sources was principally based on the modal characteristics of the distributions and further post-processing analyses including: (1) the daily trends of factor contributions (Figure 8); (2) the investigation of the source directionality by mean of polar plot and polar annulus analyses (Figure 8); (3) the results of Spearman rank correlations ( $\rho$ ) with other measured pollutants (Table 2) and (4) cross-correlation functions (CCFs) among variables and calculated at  $\pm 24$  h lag time using hourly averaged data or with higher time resolution (5 min) and within  $\pm 3$  h lag time for PMF source contributions and BC data (Figure 9).

The *first factor* includes most of the particles in the nucleation range ( $< 25$  nm), exhibits a sharp mode in the number distribution at 15-20 nm and makes the largest contribution to the total PNC (43.8%, confidence interval at 95% based on 200 BS runs (c.i.<sub>95</sub>) between 43.4 and 44.1%). However, its contribution to the volume distribution is  $\sim 1\%$ . This factor shows significant ( $p < 0.001$ ) but weak ( $0.35 < \rho < 0.6$ ) positive correlations with NO (but not NO<sub>2</sub>), OX, solar irradiance, air temperature and exhibits an evident diurnal variation peaking at 1 pm and higher levels during the afternoon. The polar plot analysis (Figure 8) indicates enhanced levels when winds blow from the SW and SE quadrants: whilst the increase from the SE quadrant arises for high wind speeds ( $> 5$  m s<sup>-1</sup>) towards the airfield, the increase in the SW quadrant occurs for lower speeds (3–5 m s<sup>-1</sup>).

The polar annulus analysis indicates that the higher concentrations are for winds blowing from S to SW at 12 noon-4pm. This behaviour is consistent with the location of several anthropogenic sources in the study area which can contribute to particles in the nucleation range, i.e. the road traffic in the urban area of Mestre (toward SW), the stack emissions from the industrial area (SW), shipping in Venice and its tourist harbour (S) and the airport activities and aircraft movements (SE). In this



context, particles peaking in the nucleation range have been observed for multiple anthropogenic sources: (i) fresh diesel engines (Shi and Harrison, 1999), (ii) diesel-equipped boats at high engine loads (Petzold et al., 2010), (iii) coal-fired power plants (Nielsen et al., 2002; Liu et al., 2010) aircraft (Anderson et al., 2005; Kinsey et al., 2010; Mazaheri et al., 2013; Lobo et al., 2015). However, particles in this size range may also originate from photochemically-driven nucleation processes. The profile for this factor relates well to the shapes grouped in the cluster 5 in the *k*-means cluster analysis (midday nucleation events). The polar plot for this factor (Figure 8) also shows the highest intensity in areas of the plot showing the lowest PM<sub>2.5</sub> concentrations (Figure 3). This is consistent with nucleation being favoured by a low condensation sink (Dall'Osto et al., 2013).

Beside the number of potential sources for this factor, the daily profile (Figure 8) shows a sharp peak at noon-2pm which is strongly related to the solar irradiance and well matches with the hourly counts of cluster 5, but also bears some similarity to aircraft movements (Figure 2) or road traffic rush hours. Aircraft takeoffs start before 6am, when the contribution of this factor is still low. Moreover, the maximum average values shown in the polar and annulus plots at noon-2pm are towards the SW, which is not consistent with a main origin from the airfield.

Results of a subsequent study give further insights for interpreting the first factor. A similar sampling campaign was carried out in July 2014 at a kerbside site in the urban area of Mestre using a similar set of instruments (SMPS, aethalometer). Preliminary results of this study are provided as supplementary material: Figure SI6 shows the map of the sampling location, while Figure SI7 reports the “nucleation factor” extracted by applying PMF analysis to SMPS data. These results show an identical size distribution (particles peaking at 15-20 nm) with a similar daily pattern (main peak at noon-1pm followed by a second minor peak at 6-7am). However, the polar plot analysis significantly differs showing strong increases for winds blowing from the SE, i.e. the direction of

the industrial zone. Since the kerbside site is located 9.5 km WSW from VCE and weather conditions were very similar (summer sea/land breeze regime), an origin of factor 1 from airport activities is not consistent with the results. An origin from the industrial zone is plausible. As already reported, a large coal-fired power plant and a an oil refinery are located in the industrial area of Porto Marghera and both installations are potential sources of particles in the nucleation range (Nielsen et al., 2002; Liu et al., 2010; Cheung et al., 2012) and SO<sub>2</sub>. Emission inventories for 2010 (ARPAV – Regione Veneto, 2015) reported that combustion in energy and transformation industries accounts for ~72% of total SO<sub>2</sub> emissions in the Venice Province. It has been reported that the probability of nucleation is increased by elevated SO<sub>2</sub> concentrations (e.g., Stanier et al., 2004) and a 13 year-long monitoring of airborne pollutants conducted in Mestre (Masiol et al., 2014b) reported evident peaks of SO<sub>2</sub> for winds blowing from the industrial zone. A large influence of oil refineries and/or coal-fired power plants upon the particle number concentrations in the nucleation range have been observed in many parts of the world (e.g., Stevens et al., 2012; Cheung et al., 2012; González and Rodríguez, 2013).

All of these insights support the interpretation of factor 1 as mainly driven by photochemical nucleation processes occurring in the atmosphere (Seinfeld and Pandis, 2006; Zhang et al., 2011) probably including gas-to-particle conversion of SO<sub>2</sub>. CCFs (Figure 9) well depict the relationship between this factor and solar irradiation: a short delay of the highest positive correlations at +1/+2 h lags may be attributed to the time needed for the growth of nucleated particles into the measured size range. However, beside its main probable origin from photochemical nucleation of SO<sub>2</sub>, the directional analysis (Figure 8) further suggests that this factor might also be also secondarily associated with locally-emitting primary anthropogenic sources.

Since the sampling site is located downwind of major combustion sources during sea breeze regimes, particles arising from the urban area are sampled on timescales of several minutes after

emission and, then, may undergo to a substantial evaporative shrinkage resulting in a shift toward smaller sizes. The condensation/evaporation/dilution processes have been demonstrated to be major mechanisms in altering aerosol size distributions after primary particles in the nucleation range are emitted in the atmosphere (Zhang et al., 2004; Harrison et al., 2016); this effect has been observed in heavily developed urban areas, such as London (Dall'Osto et al., 2011). In addition, the polar plot for factor 1 also shows minor increases towards the airfield for strong winds. The sulphur content in jet fuel is limited to 3000 ppm and is commonly reported within the range 300–1100 ppm (Masiol and Harrison, 2014, and reference therein), which is approximately 30-100 times higher than that for automotive fuels (<10 ppm). Consequently, aircraft emissions are a high potential source of SO<sub>2</sub> and may secondarily contribute to this factor under some particular circumstances.

The summary, although this factor could consist of a few distinct sources resulting in poorly resolved PMF solutions, its fingerprint remains similar for solutions of up to 10 factors, demonstrating its structural robustness and the lack of potential artefacts upon the PMF solution. As a consequence, the hypothesis of multiple-source attribution for nucleation particles is plausible and it is impossible to assign to a specific one with certainty. However, the temporal profile and the fact that the same source profile was found in another site in the area and affected by different emission scenarios is very consistent with a nucleation source driven by regional processes and the most significant sources of sulphur dioxide in the area.

The *second factor* is made up of ultrafine particles in the nucleation range (20 to 100 nm) with a clear mode at 35–40 nm for the number distribution, and which accounts for 25.5% (c.i.<sub>95</sub> 25.3–25.9%) of particle number. Its contribution to the volume distribution is low (~5%) and peaks at 80 and 500 nm. Several observations link this factor to road traffic: (i) correlation analysis shows significant moderate positive associations with NO<sub>2</sub> ( $\rho=0.44$ ) and BC ( $\rho=0.41$ ), which are pollutants primarily emitted by road traffic (mainly diesel); (ii) such correlations have maxima at 0

h lag, suggesting covariant sources (Figure 9); (iii) the diurnal variations reveal a typical cycle common to traffic-related sources (morning and evening rush traffic hours); (iv) the directional analysis shows increased levels when air masses move from the main populated sectors of the mainland, i.e. the urban area of Mestre (SW), and several main roads towards the N and (v) the factor profile very similar to the cluster 1 (road traffic) extracted by the *k*-mean cluster analysis. It is extensively reported that particles in the size range of factor 2 may originate from the dilution of diesel exhaust emissions (Charron and Harrison, 2003; Janhäll et al., 2004; Ntziachristos et al., 2007; Harrison et al., 2011) as well as from gasoline-powered cars (Wehner et al., 2009; Huang et al., 2013). Similar factor profiles have been also reported in the literature for road traffic (e.g., Yue et al., 2008; Constabile et al., 2009; Harrison et al., 2011).

However, the polar plot analysis also shows increased levels for winds blowing from S, i.e. the direction of the historic city centre of Venice and its passenger terminal and for high wind regimes from SSE, i.e. toward the Lido inlet, a main entrance of cruise ships into the Lagoon of Venice. A number of studies have associated particles in this size range with marine traffic. Jonsson et al. (2011) reported that emissions from cargo and passenger ships peak at ~35 nm; Healy et al. (2009) observed ship exhaust particle number distributions with a maximum at approximately 50 nm; Kasper et al. (2007) observed mean diameters of particles at 20–40 nm for 2-stroke marine diesel engines; Petzold et al. (2010) associated particles with modes at 40–60 nm with a serial 4-stroke marine diesel engine at 10–50% engine load; Kivekäs et al. (2014) observed that the contribution of ship traffic to PNC downwind of a major shipping lane consists of number distributions peaking at ~40 nm. The same results were also reported by Lyyränen et al. (1999), who investigated the mechanisms of particle formation during combustion within marine diesel engines affected by hot corrosion and erosion. In the light of this, besides road traffic, factor 2 can be also linked to the marine traffic emissions from ships, waterbuses and boats of public or private transport services, which are commonly equipped with marine diesel engines. Currently, the contribution of the Port of

Venice to the levels of PM is heavily debated (Contini et al., 2015) and information on the emissions from waterbuses and the private boat fleet is still lacking (Pecorari et al., 2013a). Factor 2 was interpreted as road+shipping traffic, mainly due to diesel engine emissions.

The *third factor* shows a main mode in the number distribution at 80 nm and a second mode in the nucleation range, which seems to extend beyond the lower limit of particle detection of the SMPS (14.6 nm). Three modes in the volume distribution are found at approx. 200, 500 nm and 5  $\mu$ m. Its contributions to the particle number and volume are 20.3% (c.i.<sub>95</sub> 20.1-20.5%) and 19.6%, respectively. This factor lacks relevant correlations with other air pollutants and its diurnal cycle is relatively constant through the early part of the day, with a strong decrease in the early afternoon following the increased wind speeds due to the sea breezes. Several studies available from the current literature report that aircraft engine emissions show a main mode in the nucleation range (Masiol and Harrison, 2014, and references therein; Lobo et al., 2015). However, despite the particle size profile of factor 3 differing from those commonly reported in the literature for aircraft emissions, there are a number of reasons for attributing this factor to the airport emissions:

- The polar plot exhibits the main contributions when air masses blow from the airfield (E to SSE) and from the main airport terminal (NE), while the polar annulus clearly shows that maximum levels for winds blowing from the airfield are reached in the central hours of the day, i.e. during the busy airport hours. No other factors show polar plots consistent with aircraft emissions.
- Some studies also report the presence of a second mode in the accumulation range for aircraft exhausts (Kinsey et al., 2010; Lobo et al., 2012; Mazaheri et al. 2013). For example, in a study conducted at the Brisbane airport (Australia), Mazaheri et al. (2009) investigated a total of 283 individual aircraft plumes during landing and takeoff (LTO) cycles and reported accumulation modes between 40 and 100 nm, more pronounced in particle number size distributions during takeoffs. These findings are also consistent with Herndon et al. (2008), who studied the emissions from in-use commercial aircraft engines downwind of operational taxi- and runways at

Hartsfield-Jackson Atlanta airport (USA) and reported the presence of a mode at ~65 nm

associated with takeoff plumes and a smaller mode at ~25 nm associated with idle. Comparing the profile of factor 3 with clustering results, it can be noted that it fits profiles for both cluster 2 and 4 (aircraft and airport-related shapes). In particular, looking at the diurnal variations, factor 3 seems more related with cluster 4 than with cluster 2. Although factor 3 lacks a main peak in the nucleation range, its fingerprint (Figure 7) shows the presence of a significant second mode for particles below 14 nm, which may represent the main peak in the nucleation range reported in the literature for aircraft emissions. An apparent shift towards smaller particle sizes can be attributed to evaporative shrinkage of particles before the exhaust plumes reached the sampling site (Dall'Osto et al., 2011; Harrison et al., 2016). In this context, the total number of particles attributed by our study to the aircraft exhaust emissions will be underestimated because the lower limit of detection of SMPS curtails this second peak below 14 nm.

In addition to the main exhaust emissions from aircraft engines, there is some evidence suggesting that this factor can also be related to supplementary contributions from other on-airport sources: the high concentrations observed for winds blowing from the main terminal (ENE) suggest a supplementary contribution from the aircraft APUs. Moreover, the peaks in particle volume at 500 nm and 5  $\mu\text{m}$  can be tentatively attributed to the brake dust and tyre wear during landing and to the dust resuspension due to the turbulence created by the aircraft movements, respectively. Factor 3 was hence attributed to the primary emissions from the airport.

The *fourth factor* is a minor contributor to PNC (5.9%, c.i.<sub>95</sub> 5.8-6.1), but accounts for the main percentage of the volume distribution (41%). It has two modes in the number distribution (30 and 200 nm) and a main mode in the volume distribution (400 nm). Polar plot analysis does not reveal any significant directionality toward specific local sources, but shows a marked boost during wind calm hours ( $\rho_{\text{wind speed}} = -0.54$ ) and low winds from the NNE. The daily pattern is the mirror image

of the air temperature, and it is positively correlated with NO<sub>2</sub> (but not with NO), PM<sub>2.5</sub> and BC and negatively correlated with O<sub>3</sub>, OX and SO<sub>2</sub>. The factor 4 can be related to the cluster 3 (nighttime pollution): they match for the 30 nm peak and they show the same diurnal patterns. These results raise the following issues: (i) the higher levels reached in calm and low wind periods may suggest that the origin of the factor is local rather than external or linked to regional transport; (ii) an origin from the airport can be excluded because of the diurnal profile (very limited airport traffic recorded overnight); (iii) the directionality toward NNE, where there are no significant emission sources, may indicate that such a factor is not linked to freshly emitted pollutant. The peak intensity during the nighttime and the significant, but weak, association with NO<sub>2</sub> are highly consistent with the chemistry driving the heterogeneous reactions of N<sub>2</sub>O<sub>5</sub> and NO<sub>3</sub> on aerosol surfaces (Seinfeld and Pandis, 2006; Bertram and Thornton, 2009; Brown and Stutz, 2012). This process has been observed in many polluted areas (e.g., Fine et al., 2008; Wang et al., 2009). In particular, Dall'Osto et al. (2009) observed that most nitrate particles in London are: (i) locally produced in urban locations during nighttime; (ii) mainly present in particles smaller than 300 nm and (iii) internally mixed with sulphate, ammonium, elemental and organic carbon. Therefore, this factor clearly depicts the condensation of secondary nitrate on pre-existing particles occurring overnight and enhanced by the air temperatures below 20°C. The analysis of CCF (Figure 9) confirms this interpretation by revealing a delay of about 2 h in maximum negative correlations with ambient temperature, which is likely linked to the time needed for the heterogeneous reactions on the surface of particles. Moreover, it would be expected that nitrate-containing particles can subsequently undergo evaporation during daytime. This latter interpretation relates well to a recent study by Squizzato et al. (2013), who reported low levels of PM<sub>2.5</sub>-bound nitrate in Venice during the warm season because of the partitioning of nitrate towards the gas-phase.

Further information can be extracted by analysing this factor. The high correlation with BC ( $\rho=0.64$  with maximum correlations at 0 h lags) suggests that BC particles have a key role in the formation



processes by acting as condensation nuclei for nitrate aerosol. BC is a primary pollutant and is therefore directly emitted from specific combustion sources: in the study area principally industries (mainly coal power plant), shipping and traffic. However, none of these primary sources are located toward the NNE. This correlation is mostly driven by the concurrent effects of the nocturnal circulation (prevalent winds blowing from the NNE) and the lower mixing layer height reached in the coldest nighttime hours (typically at 6am). In the warmest season, the mixing height over the study area may reach 1 km or more during daytime, allowing a greater dispersion of pollutants emitted at the ground, whereas it drops down to below 100 m or less during night (Pecorari et al., 2013b). Therefore it can be speculated that locally-emitted BC particles and  $\text{NO}_x$  undergo a wide dispersion within the expanded mixing layer during the daytime and move toward the mainland because of the sea breezes. Overnight, the reduction of the mixing layer height restricts BC and nitrogen oxides emissions to a layer close to ground level. In this scenario, both the reduction in air temperatures and the increased concentrations of  $\text{NO}_x$  (Figure 2b) potentially boost the formation of nitrate aerosol in the particle-phase on BC nuclei.

The last two factors show main super-micrometre modes for the volume distribution, respectively at 2-3 and 4-6  $\mu\text{m}$ . Their contributions to the total particle volume concentrations are 21.1% and 12.2%, respectively, while their shares of PNC are negligible (3 and 1.5%, respectively). Apparently, both factors also show increased levels with high winds blowing from the first NE sector and diurnal cycles inverse to the air temperature. However, despite most factors showing repetitive or cyclic daily variations, *factor 5* does not present a regular diurnal pattern, but exhibits two relatively short periods with very high contributions: 18-19 and 23-24 May. This result may indicate that it is not necessarily linked with local stationary sources and not strongly affected by micro- or meso-scale weather conditions, such as breezes. Consequently, the potential origin of this factor was investigated through the concentration weighted trajectory (CWT) analysis of the back-trajectories. Details of the adopted method are provided in Hsu et al. (2003). Results reveal a



potential regional origin from Central Italy (Figure S18), but also increased levels when air masses move from some populated areas of Central Europe. The best interpretation for this factor is therefore the regional/transboundary pollution transport across Italy and/or Europe.

Data analysis of *factor 6* shows increased levels for strong winds blowing from the NE sector and higher levels in the colder hours of the day. Super-micrometre particles are likely emitted from non-combustion sources. The daily cycle is very similar to that of nighttime nitrate (factor 4), BC and NO<sub>2</sub>, but no correlations are significantly high with those variables. On the contrary, factor 6 clearly shows weak negative correlations with O<sub>3</sub>, OX, wind speed, solar irradiance and air temperature. Strong winds from the NNE bring air masses from agricultural fields as well as from some places in the surroundings of the airport affected by work during the sampling campaign. Consequently, the most plausible interpretation for factor 6 is the local resuspension of large dust particles, presumed to be of crustal origin. The diurnal pattern is explained by the fact that land breezes occur at nighttime, only linking source areas to the sampling site at this time of day.

### 3.4 Potential Sources of Black Carbon

Similar to PMF factor 4, BC levels peak at 6-7am (Figures 2 and 8), when ambient temperature drops to the daily minimum. The analysis of the polar plot for BC (Figure 3) does not reveal substantial increases of concentration in any direction, but a marked rise in levels during calm wind periods. An estimation of the relative contributions of local sources upon the BC levels was then made by comparing data for winds blowing from differing sectors. Six sectors were identified according to the location of the main sources of the study area: (i) the urban area of Mestre as representative of traffic-related emissions; (ii) the main industrial zone of Porto Marghera; (iii) Venice as representative of urban emissions and shipping; (iv) the Island of Murano for glassmaking emissions; (v) the VCE airfield comprising runway, taxiway and the main terminals and (vi) remaining sector. Selected sectors and polar annulus results are provided in Table 3 and

Figure SI3, respectively. Data were also filtered for wind speed  $>1 \text{ m s}^{-1}$  to remove wind calm periods. Results (Figure 10) show that the BC levels are higher when air masses arise from the 'other direction' sector, while they are almost constant for sectors indicative of each specific local anthropogenic source. This result is quite unexpected as soot particles are known to be emitted by most combustion sources in the area, e.g., road traffic (Pant and Harrison, 2013), aircraft (Masiol and Harrison, 2014), and ships (Lack and Corbett, 2012), while emissions from wood combustion due to domestic heating and open burning are negligible in warm periods. During daytime, none of the local sources seems to have a dominant role in influencing the levels of atmospheric soot, while the nocturnal circulation (slow winds prevalently from NNE) and the lower mixing layer height (ca. 100 m) at nighttime restricts soot particles to the surface layer close to the ground.

#### 4. CONCLUSIONS

This study was carried out at an international airport located in an area with a very complex emission scenario with the aim of detecting and apportioning the most probable sources of particles and black carbon. The main results can be summarised as follows:

- the fingerprint of aircraft emissions on the PNSD sampled in real ambient conditions reveals a main mode at approx. 80 nm and a second mode in the nucleation range below the lower limit for particle detection of the SMPS ( $<14 \text{ nm}$ ). Air traffic contributes about 22% of PNC, but does not contribute significantly to the mass concentrations of black carbon. However, the size distribution fingerprint could be affected by evaporative processes which have shifted the particle size below 14 nm and, thus, the total amount of particles emitted by the airport could be underestimated;
- nucleation particles with a mode at 15-20 nm are the main contributors to PNC (44%) and may be linked to both photochemical nucleation from precursor gases and the evolution of primary particles emitted by several combustion processes and undergoing condensation/evaporation/dilution processes after emission. Cluster analysis has helped to

identify and quantify the midday nucleation episodes, which were recorded for about 40% of sampling days;

- the emissions of road traffic from the main urban area and shipping traffic around the city of Venice contributes to ~26% of PNC (mode at 35-40 nm);
- Coarse particles originated from nighttime nitrate formation and from resuspension advected by regional transport are the main contributors to the particle volume concentrations and, therefore, mass concentrations, as clearly indicated by significant positive correlations with  $PM_{2.5}$ ;
- levels of black carbon are strongly associated with the dynamics of the mixing layer, while no specific local sources can be identified as dominant in the study area. BC also has an important role by providing condensation nuclei for nighttime secondary nitrate aerosol formation.

In summary, sources related to transport sectors are amongst the largest contributors to local air pollutant concentrations. Beside aircraft traffic, airports are often located near major cities and attract large volumes of road traffic, which are additive to the local pollution. Furthermore, micro- and meso-scale meteorology may move, mix and transform emitted primary pollutants. It is therefore very difficult to differentiate between pollutants arising from airport operations and those from other local sources. The approaches proposed in this study have successfully identified and apportioned the main potential sources in an area affected by a complex emission scenario and the results can be utilised to plan local air pollution control measures.

This study is the first to apply cluster analysis and receptor modelling techniques for assessing the sources of wide-range particle size spectra at an international airport. Although such techniques are widely used to detect and quantify the sources of airborne particles (both for mass and number concentrations), their application to data collected near airports, or even inside the airfields, is still very limited. There are a number of reasons for this as studies at airports must face several issues:

- (i) the need of specific authorisations to enter the airport area for carrying chemical substances

and/or radioactive sources required by some scientific equipment; (ii) the space and time allowed for research is strictly limited for compliance with the strong security standards of airports; (iii) the positioning of sampling sites is also restricted to fulfil security standards. For these reasons, limitations affected this study, such as the length of the sampling campaign and the location of the sampling site. They both represent the best compromise between stringent safety measures for flights and scientific investigation.

## ACKNOWLEDGEMENTS

The authors gratefully acknowledge: (i) the European Union for funding the Marie Curie Intra-European Fellowship for career development to M. Masiol through the project entitled 'Chemical and Physical Properties and Source Apportionment of Airport Emissions in the context of European Air Quality Directives (Project CHEERS, call: FP7-PEOPLE-2012-IEF, proposal no. 328542); (ii) SAVE S.p.A. (Davide Bassano, Saverio Sollecito) for logistic, technical support and for supplying aircraft movement data; (iii) Ente Zona Industriale di Porto Marghera ([www.entezona.it](http://www.entezona.it)) for providing some pollutant and weather data; (iv) Stefania Squizzato (Ca' Foscari University of Venice) and Gianni Formenton (ARPAV) for the valuable exchange of information and discussion. The authors gratefully acknowledge the NOAA Air Resources Laboratory (ARL) for the provision of the HYSPLIT transport and dispersion model used in this publication.

## REFERENCES

- Anderson, B.E., Branham, H.-S., Hudgins, C.H., Plant, J.V., Ballenthin, J.O., Miller, T.M., Viggiano, A.A., Blake, D.R., Boudries, H., Canagaratna, M., Miake-Lye, R.C., Onasch, T., Wormhoudt, J., Worsnop, D., Brunke, K.E., Culler, S., Penko P., Sanders, T., Han, H.-S., Lee, P., Pui, D.Y.H., Thornhill, K.L., Winstead, E.L., 2005. Experiment to Characterize Aircraft Volatile Aerosol and Trace-Species Emissions (EXCAVATE). NASA/TM-2005-213783. National Aeronautics and Space Administration, Hampton, VA. August 2005.
- ARPAV, 2014. INEMAR Veneto, Inventario emissioni in atmosfera: emissioni in Regione Veneto, edizione 2007/8 - dati definitivi. ARPA Veneto and Regione Veneto. Available from: <http://89.96.234.242/inemar/webdata/main.seam> (last accessed on January 2014).
- ARPAV – Regione Veneto, 2015. INEMAR VENETO 2010 - Inventario Regionale delle Emissioni in Atmosfera in Regione Veneto, edizione 2010 – dati in versione definitiva. ARPA Veneto - Osservatorio Regionale Aria, Regione del Veneto - Dipartimento Ambiente, Sezione Tutela Ambiente, Settore Tutela Atmosfera.
- Beddows, D.C.S., Dall'Osto, M., Harrison, R.M., 2009. Cluster analysis of rural, urban and curbside atmospheric particle size data. *Environ. Sci. Technol.* 43, 4694–4700.
- Beddows, D.C.S., Dall'Osto, M., Harrison, R.M., 2010. An enhanced procedure for the merging of atmospheric particle size distribution data measured using electrical mobility and time-of-flight analysers. *Aerosol Sci. Technol.* 44, 930–938.
- Beddows, D.C.S., Dall'Osto, M., Harrison, R. M., Kulmala, M., Asmi, A., Wiedensohler, A., Laj, P., Fjaeraa, A.M., Sellegri, K., Birmili, W., Bukowiecki, N., Weingartner, E., Baltensperger, U., Zdimal, V., Zikova, N., Putaud, J.-P., Marinoni, A., Tunved, P., Hansson, H.-C., Fiebig, M., Kivekäs, N., Swietlicki, E., Lihavainen, H., Asmi, E., Ulevicius, V., Aalto, P. P., Mihalopoulos, N., Kalivitis, N., Kalapov, I., Kiss, G., de Leeuw, G., Henzing, B., O'Dowd, C., Jennings, S. G., Flentje, H., Meinhardt, F., Ries, L., Denier van der Gon, H. A. C., Visschedijk, A. J. H., 2014. Variations in tropospheric submicron particle size distributions across the European continent 2008–2009. *Atmos. Chem. Phys.* 14, 4327–4348.
- Beelen, R., Raaschou-Nielsen, O., Stafoggia, M., Andersen, Z.J., Weinmayr, G., Hoffmann, B., Wolf K., Samoli, E., Fischer, P., Nieuwenhuijsen, M., Vineis, P., Xun, W.W., Katsouyanni, K., Dimakopoulou, K., Oudin, A., Forsberg, B., Modig, L., Havulinna, A.S., Lanki, T., Turunen, A., Oftedal, B., Nystad, W., Nafstad, P., De Faire, U., Pedersen, N.L., Östenson, C.G., Fratiglioni, L., Penell, J., Korek, M., Pershagen, G., Thorup Eriksen, K., Overvad, K., Ellermann, T., Eeftens, M., Peeters, P.H., Meliefste, K., Wang, M., Bueno-de-Mesquita, B., Sugiri, D., Krämer, U., Geinrich, J., de Hoogh, K., Key, T., Peters, A., Hampel, R., Concin, H., Nagel, G., Ineichen, A., Schaffner, E., Probst-Hensch, N., Künzli, N., Schindler, C., Schikowski, T., Adam, M., Phuleria, H., Vilier, A., Clavel-Chapelon, F., Declercq, C., Grioni, S., Krogh, V., Tsai, M.-Y., Ricceri, F., Sacerdote, C., Galassi, C., Migliore, E., Ranzi, A., Cesaroni, G., Badaloni, C., Forastiere, F., Tamayo, I., Amiano, P., Dorronsoro, M., Katsoulis, M., Trichopoulou, A., Brunekreef, B., Hoek, G., 2014. Effects of long-term exposure to air pollution on natural-cause mortality: an analysis of 22 European cohorts within the multicentre ESCAPE project. *Lancet* 383, 785–795.
- Belis, C.A., Larsen, B.R., Amato, F., El Haddad, I., Favez, O., Harrison, R.M., Hopke, P.K., Nava, S., Paatero, P., Prévôt, A., Quass, U., Vecchi, R., Viana, M., 2014. European guide on air pollution source apportionment with receptor models. JRC Reference Reports EUR26080 EN

- Bertram, T. H., Thornton, J. A., 2009. Toward a general parameterization of N<sub>2</sub>O<sub>5</sub> reactivity on aqueous particles: the competing effects of particle liquid water, nitrate and chloride. *Atmos. Chem. Phys.* 9, 8351-8363.
- Brines, M., Dall'Osto, M., Beddows, D.C.S., Harrison, R. M., Querol, X., 2014. Simplifying aerosol size distributions modes simultaneously detected at four monitoring sites during SAPUSS. *Atmos. Chem. Phys.* 14, 2973-2986.
- Brines, M., Dall'Osto, M., Beddows, D., Harrison, R., Gómez-Moreno, F., Núñez, L., Artíñano, B., Costabile, F., Gobbi, G., Salimi, F., 2015. Traffic and nucleation events as main sources of ultrafine particles in high-insolation developed world cities. *Atmos. Chem. Phys.* 15, 5929-5945.
- Brown, S.S., Stutz, J., 2012. Nighttime radical observations and chemistry. *Chem. Soc. Rev.* 41, 6405–6447.
- Brown, S.G., Eberly, S., Paatero, P., Norris, G.A., 2015. Methods for estimating uncertainty in PMF solutions: Examples with ambient air and water quality data and guidance on reporting PMF results. *Sci.Total Environ.* 518, 626-635.
- Carslaw, D.C., Ropkins, K., 2012. openair - an R package for air quality data analysis. *Environ. Model. Softw.* 27-28, 52-61.
- Carslaw, D.C., Beevers, S.D., Ropkins, K., Bell, M.C., 2006. Detecting and quantifying aircraft and other on-airport contributions to ambient nitrogen oxides in the vicinity of a large international airport. *Atmos. Environ.* 40, 5424–5434.
- Carslaw, D.C., Beevers, S.D., Bell, M.C., 2007. Risks of exceeding the hourly EU limit value for nitrogen dioxide resulting from increased road transport emissions of primary nitrogen dioxide. *Atmos. Environ.* 41, 2073-2082.
- Charron, A., Harrison, R.M., 2003. Primary particle formation from vehicle emissions during exhaust dilution in the roadside atmosphere. *Atmos. Environ.* 37, 4109–4119.
- Chen, J.P., Tsai, T.S., Liu, S.C., 2011. Aerosol nucleation spikes in the planetary boundary layer. *Atmos. Chem. Phys.* 11, 7171-7184.
- Cheung, H. C., Morawska, L., Ristovski, Z. D., and Wainwright, D., 2012. Influence of medium range transport of particles from nucleation burst on particle number concentration within the urban airshed. *Atmos. Chem. Phys.* 12, 4951-4962.
- Costabile, F., Birmili, W., Klose, S., Tuch, T., Wehner, B., Wiedensohler, A., Franck, U., König, K., Sonntag, A., 2009. Spatio-temporal variability and principal components of the particle number size distribution in an urban atmosphere. *Atmos. Chem. Phys.* 9, 3163-3195.
- Contini, D., Gambaro, A., Donato, A., Cescon, P., Cesari, D., Merico, E., Citron, M., 2015. Inter-annual trend of the primary contribution of ship emissions to PM 2.5 concentrations in Venice (Italy): Efficiency of emissions mitigation strategies. *Atmos. Environ.* 102, 183-190.
- Cyrys, J., Eeftens, M., Heinrich, J., Ampe, C., Armengaud, A., Beelen, R., Bellander, T., Beregszaszi, T., Birk, M., Cesaroni, G., Cirach, M., de Hoogh, K., De Nazelle, A., de Vocht, F., Declercq C., Dedele, A., Dimakopoulou, K., Eriksen, K., Galassi, C., Grauleviciene, R., Grivas, G., Gruzjeva, O., Hagenbjörk Gustafsson, A., Hoffmann, B., Iakovides, M., Ineichen, A., Krämer, U.,



- Lanki, T., Lozano, P., Madsen, C., Meliefste, K., Modig, L., Mölterm, A., Mosler, G., Nieuwenhuijsen, M., Nonnemacher, M., Oldenwening, M., Peters, A., Pontet, S., Probst-Hensch, N., Quass, U., Raaschou-Nielsen, O., Ranzi, A., Sugiri, D., Stephanou, E.G., Taimisto, P., Tsai, M.-Y., Vaskövi, E., Villani, S., Wang, M., Brunekreef, B., Hoek, G., 2012. Variation of NO<sub>2</sub> and NO<sub>x</sub> concentrations between and within 36 European study areas: Results from the ESCAPE study. *Atmos. Environ.* 62, 374–390.
- Dal Maso, M., Kulmala, M., Riipinen, I., Wagner, R., Hussein, T., Aalto, P.P. Lehtinen, K.E., 2005. Formation and growth of fresh atmospheric aerosols: eight years of aerosol size distribution data from SMEAR II, Hyytiälä, Finland. *Boreal Env. Res.* 10(5), p.323.
- Dall'Osto, M., Harrison, R.M., Coe, H., Williams, P.I., Allan, J.D., 2009. Real time chemical characterization of local and regional nitrate aerosols. *Atmos. Chem. Phys.* 9, 3709-3720.
- Dall'Osto, M., Thorpe, A., Beddows, D.C.S., Harrison, R.M., Barlow, J.F., Dunbar, T., Williams, P.I., Coe, H., 2011. Remarkable dynamics of nanoparticles in the urban atmosphere. *Atmos. Chem. Phys.* 11, 6623-6637.
- Dall'Osto, M., Beddows, D.C.S., Pey, J., Rodriguez, S., Alastuey, A., Harrison, Roy M., Querol, X., 2012. Urban aerosol size distributions over the Mediterranean city of Barcelona, NE Spain. *Atmos. Chem. Phys.* 12, 10693-10707.
- Dall'Osto, M., Querol, X., Alastuey, A., O'Dowd, C., Harrison, R.M., Wenger, J. and Gómez, Moreno, F.J., 2013. On the spatial distribution and evolution of ultrafine particles in Barcelona. *Atmos. Chem. Phys.* 13, 741-759.
- Dodson, R.E., Houseman, E.A., Morin, B., Levy, J.I., 2009. An analysis of continuous black carbon concentrations in proximity to an airport and major roadways. *Atmos. Environ.* 43, 3764-3773.
- Fine, P.M., Sioutas, C., Solomon, P.A., 2008. Secondary particulate matter in the United States: Insights from the Particulate Matter Supersites Program and related studies. *JAWMA* 58, 234–253.
- Fiore, A.M., Naik, V., Spracklen, D.V., Steiner, A., Unger, N., Prather, M., Bergmann, D., Cameron-Smith, P.J., Cionni, I., Collins, W.J., Dalsøren, S., Eyring, V., Folberth, G.A., Ginoux, P., Horowitz, L.W., Josse, B., Lamarque, J.-F., MacKenzie, I.A., Nagashima, T., O'Connor, F.M., Righi, M., Rumbold, S.T., Shindell, D.T., Skeie, R.B., Sudo, K., Szopa, S., Takemura, T., Zeng, G., 2012. Global air quality and climate. *Chem. Soc. Rev.* 41, 6663-6683.
- Friend, A.J., Ayoko, G.A., Jager, D., Wust, M., Jayaratne, E.R., Jamriska, M. Morawska, L., 2013. Sources of ultrafine particles and chemical species along a traffic corridor: comparison of the results from two receptor models. *Environ. Chem.* 10(1), 54-63.
- González, Y., Rodríguez, S., 2013. A comparative study on the ultrafine particle episodes induced by vehicle exhaust: A crude oil refinery and ship emissions. *Atmos. Res.* 120, 43-54.
- Grice, S., Stedman, J., Kent, A., Hobson, M., Norris, J., Abbott, J., Cooke S., 2009. Recent trends and projections of primary NO<sub>2</sub> emissions in Europe. *Atmos. Environ.* 43, 2154-2167.
- Hamed, A., Joutsensaari, J., Mikkonen, S., Sogacheva, L., Dal Maso, M., Kulmala, M., Cavalli, F., Fuzzi, S., Facchini, M. C., Decesari, S., Mircea, M., Lehtinen, K. E. J., Laaksonen, A., 2007. Nucleation and growth of new particles in Po Valley, Italy. *Atmos. Chem. Phys.* 7, 355-376.

- Harrison, R.M., Jones, A.M., Beddows, D.C.S., Dall'Osto, M., Nikolova, I., 2016. Evaporation of traffic-generated nanoparticles during advection from source. *Atmos. Environ.* 125, 1-7.
- Harrison, R.M., Beddows, D.C.S., Dall'Osto, M., 2011. PMF Analysis of wide-range particle size spectra collected on a major highway. *Environ. Sci. Technol.* 45, 5522–5528.
- Heal, M. R., Kumar, P., Harrison, R. M., 2012. Particles, air quality, policy and health. *Chem. Soc. Rev.* 41, 6606-6630.
- Healy, R.M., O'Connor, I.P., Hellebust, S., Allanic, A., Sodeau, J.R., Wenger, J.C., 2009. Characterisation of single particles from in-port ship emissions. *Atmos. Environ.* 43, 6408-6414.
- Herndon, S.C., Jayne, J.T., Lobo, P., Onasch, T.B., Fleming, G., Hagen, D.E., Whitefield, P.D., Miake-Lye, R.C., 2008. Commercial aircraft engine emissions characterization of in-use aircraft at Hartsfield-Jackson Atlanta International Airport. *Environ. Sci. Technol.* 42, 1877-1883.
- Hirsikko, A., Vakkari, V., Tiitta, P., Hatakka, J., Kerminen, V.-M., Sundström, A.-M., Beukes, J. P., Manninen, H.E., Kulmala, M., Laakso, L., 2013. Multiple daytime nucleation events in semi-clean savannah and industrial environments in South Africa: analysis based on observations. *Atmos. Chem. Phys.* 13, 5523-5532.
- Hopke, P.K., 2016. Review of receptor modeling methods for source apportionment. *J. Air Waste Manage. Assoc.* doi:10.1080/10962247.2016.1140693.
- Hsu, Y.K., Holsen, T.M., Hopke, P.K., 2003. Comparison of hybrid receptor models to locate PCB sources in Chicago. *Atmos. Environ.* 37, 545-562.
- Hudda, N, Gould, T., Hartin, K., Larson, T.V., Fruin, S.A., 2014. Emissions from an international airport increase particle number concentrations 4-fold at 10 km downwind. *Environ. Sci. Technol.* 48, 6628–6635.
- Hussein, T., Molgaard, B., Hannuniemi, H., Martikainen, J., Järvi, L., Wegner, T., Ripamonti, G., Weber, S., Vesala, T., Hämeri, K., 2014. Fingerprints of the urban particle number size distribution in Helsinki, Finland: Local vs. regional characteristics. *Boreal Env. Res.* 19, 1–20.
- ICAO, 2008. Environmental Protection (Annex 16), Vol. 2 – Aircraft Engine Emission, International Civil Aviation Organization, International Standards and Recommended Practices, ISBN 978-92-9231-123-0.
- Janhäll S., Jonsson Å.M., Molnár P., Svensson E.A., Hallquist M., 2004. Size resolved traffic emission factors of submicrometer particles. *Atmos. Environ.* 38, 4331–4340.
- Janssen, R.H.H., Vilà-Guerau de Arellano, J., Ganzeveld, L.N., Kabat, P., Jimenez, J.L., Farmer, D.K., van Heerwaarden, C.C., Mammarella, I., 2012. Combined effects of surface conditions. boundary layer dynamics and chemistry on diurnal SOA evolution. *Atmos. Chem. Phys.* 12, 6827-6843.
- Jonsson, Å.M., Westerlund, J., Hallquist, M., 2011. Size-resolved particle emission factors for individual ships. *Geophys. Res. Lett.* 38, L13809.
- Kasper, A., Aufdenblatten, S., Forss, A., Mohr, M., Burtscher, H., 2007. Particulate emissions from a low-speed marine diesel engine. *Aerosol Sci. Technol.* 41, 24-32.



- Keuken, M.P., Moerman, M., Zandveld, P., Henzing, J.S., Hoek, G., 2015. Total and size-resolved particle number and black carbon concentrations in urban areas near Schiphol airport (the Netherlands). *Atmos. Environ.* 104 132-142.
- Kinsey, J.S., Dong, Y., Williams, D.C., Logan, R., 2010. Physical characterization of the fine particle emissions from commercial aircraft engines during the aircraft particle emissions experiment (APEX) 1 to 3. *Atmos. Environ.* 44, 2147-2156.
- Kivekäs, N., Massling, A., Grythe, H., Lange, R., Rusnak, V., Carreno, S., Skov, H., Swietlicki, E., Nguyen, Q. T., Glasius, M., Kristensson, A., 2014. Contribution of ship traffic to aerosol particle concentrations downwind of a major shipping lane. *Atmos. Chem. Phys.* 14, 8255-8267.
- Kley, D., Kleinmann, M., Sanderman, H., Krupa, S., 1999. Photochemical oxidants: state of the science. *Environ. Pollut.* 100, 19-42.
- Kulmala, M. Kerminen, V.-M., 2008. On the formation and growth of atmospheric nanoparticles. *Atmos. Res.* 90, 132–150.
- Kulmala, M., Asmi, A., Lappalainen, H. K., Baltensperger, U., Brenguier, J.-L., Facchini, M. C., Hansson, H.-C., Hov, Ø., O'Dowd, C. D., Pöschl, U., Wiedensohler, A., Boers, R., Boucher, O., de Leeuw, G., Denier van der Gon, H. A. C., Feichter, J., Krejci, R., Laj, P., Lihavainen, H., Lohmann, U., McFiggans, G., Mentel, T., Pilinis, C., Riipinen, I., Schulz, M., Stohl, A., Swietlicki, E., Vignati, E., Alves, C., Amann, M., Ammann, M., Arabas, S., Artaxo, P., Baars, H., Beddows, D. C. S., Bergström, R., Beukes, J. P., Bilde, M., Burkhardt, J. F., Canonaco, F., Clegg, S. L., Coe, H., Crumeyrolle, S., D'Anna, B., Decesari, S., Gilardoni, S., Fischer, M., Fjaeraa, A. M., Fountoukis, C., George, C., Gomes, L., Halloran, P., Hamburger, T., Harrison, R. M., Herrmann, H., Hoffmann, T., Hoose, C., Hu, M., Hyvärinen, A., Hörrak, U., Iinuma, Y., Iversen, T., Josipovic, M., Kanakidou, M., Kiendler-Scharr, A., Kirkevåg, A., Kiss, G., Klimont, Z., Kolmonen, P., Komppula, M., Kristjánsson, J.-E., Laakso, L., Laaksonen, A., Labonnote, L., Lanz, V. A., Lehtinen, K. E. J., Rizzo, L. V., Makkonen, R., Manninen, H. E., McMeeking, G., Merikanto, J., Minikin, A., Mirme, S., Morgan, W. T., Nemitz, E., O'Donnell, D., Panwar, T. S., Pawlowska, H., Petzold, A., Pienaar, J. J., Pio, C., Plass-Duelmer, C., Prévôt, A. S. H., Pryor, S., Reddington, C. L., Roberts, G., Rosenfeld, D., Schwarz, J., Seland, Ø., Sellegri, K., Shen, X. J., Shiraiwa, M., Siebert, H., Sierau, B., Simpson, D., Sun, J. Y., Topping, D., Tunved, P., Vaattovaara, P., Vakkari, V., Veefkind, J. P., Visschedijk, A., Vuollekoski, H., Vuolo, R., Wehner, B., Wildt, J., Woodward, S., Worsnop, D. R., van Zadelhoff, G.-J., Zardini, A. A., Zhang, K., van Zyl, P. G., Kerminen, V.-M., S Carslaw, K., and Pandis, S. N., 2011. General overview: European Integrated project on Aerosol Cloud Climate and Air Quality interactions (EUCAARI) – integrating aerosol research from nano to global scales. *Atmos. Chem. Phys.* 11, 13061-13143.
- Lack, D.A., Corbett, J.J., 2012. Black carbon from ships: a review of the effects of ship speed, fuel quality and exhaust gas scrubbing. *Atmos. Chem. Phys.* 12, 3985–4000.
- Lee, D.S., Fahey, D.W., Forster, P.M., Newton, P.J., Wit, R.C.N., Lim, L.L., Owen, B., Sausen, R., 2009. Aviation and global climate change in the 21st century. *Atmos. Environ.* 43, 3520-3537.
- Liu, X., Wang, W., Liu, H., Geng, C., Zhang, W., Wang, H., Liu, Z., 2010. Number size distribution of particles emitted from two kinds of typical boilers in a coal-fired power plant in China. *Energy Fuels* 24(3), 1677-1681.

- Lobo, P., Hagen, D.E., Whitefield, P.D., 2012. Measurement and analysis of aircraft engine PM emissions downwind of an active runway at the Oakland International Airport. *Atmos. Environ.* 61, 114-123.
- Lobo, P., Hagen, D. E., Whitefield, P. D., Raper, D., 2015. PM emissions measurements of in-service commercial aircraft engines during the Delta-Atlanta Hartsfield Study. *Atmos. Environ.* 104, 237-245.
- Lyyrinen, J., Jokiniemi, J., Kauppinen, E.I., Joutsensaari, J., 1999. Aerosol characterisation in medium-speed diesel engines operating with heavy fuel oils. *J. Aerosol Sci.* 30, 771-784.
- Masiol, M., Harrison, R.M., 2014. Aircraft engine exhaust emissions and other airport-related contributions to ambient air pollution: A review. *Atmos. Environ.* 95, 409-455.
- Masiol, M., Squizzato, S., Rampazzo, G., Pavoni, B., 2014a. Source apportionment of PM<sub>2.5</sub> at multiple sites in Venice (Italy): Spatial variability and the role of weather. *Atmos. Environ.* 98, 78-88.
- Masiol, M., Agostinelli, C., Formenton, G., Tarabotti, E., Pavoni, B., 2014b. Thirteen years of air pollution hourly monitoring in a large city: Potential sources, trends, cycles and effects of car-free days. *Sci. Total Environ.* 494-495, 84-96.
- Mazaheri, M., Johnson, G.R., Morawska, L., 2009. Particle and gaseous emissions from commercial aircraft at each stage of the landing and takeoff cycle. *Environ. Sci. Technol.* 43, 441-446.
- Mazaheri, M., Bostrom, T.E., Johnson, G.R., Morawska, L., 2013. Composition and morphology of particle emissions from in-use aircraft during takeoff and landing. *Environ. Sci. Technol.* 47, 5235-5242.
- Modini, R.L., Ristovski, Z.D., Johnson, G.R., He, C., Surawski, N., Morawska, L., Suni, T., Kulmala, M., 2009. New particle formation and growth at a remote, sub-tropical coastal location. *Atmos. Chem. Phys.* 9, 7607-7621.
- Nielsen, M. T., Livbjerg, H., Fogh, C. L., Jensen, J. N., Simonsen, P., Lund, C., Poulsen, K., Sander, B., 2002. Formation and emission of fine particles from two coal-fired power plants. *Comb. Sci. Technol.* 174(2), 79-113.
- Ntziachristos, L., Ning, Z., Geller, M.D., Sioutas, C., 2007. Particle concentration and characteristics near a major freeway with heavy-duty diesel traffic. *Environ. Sci. Technol.* 41, 2223-2230.
- O'Dowd, C.D., Hoffmann, T., 2006. Coastal new particle formation: A review of the current state-of-the-art. *Environ. Chem.* 2, 245-255.
- O'Dowd, C.D., De Leeuw, G., 2007. Marine aerosol production: A review of the current knowledge. *Philos. Roy. Soc. A.* 365, 1753-1774.
- O'Dowd, C., McFiggans, G., Creasey, D. J., Pirjola, L., Hoell, C., Smith, M.H., Allan, B.J., Plane, J.M.C., Heard, D.E., Lee, J.D., Pilling, M.J., Kulmala, M., 1999. On the photochemical production of new particles in the coastal boundary layer. *Geophys. Res. Lett.* 26, 1707-1710.

- Ogulei, D., Hopke, P.K., Wallace, L.A., 2006. Analysis of indoor particle size distributions in an occupied townhouse using positive matrix factorization. *Indoor Air* 16(3), 204-215.
- Ogulei, D., Hopke, P.K., Chalupa, D.C., Utell, M.J., 2007. Modeling source contributions to submicron particle number concentrations measured in Rochester, New York. *Aerosol Sci. Technol.* 41, 179-201.
- Paatero, P., 1997. Least squares formulation of robust non-negative factor analysis. *Chemom. Intell. Lab. Syst.* 37, 23-35.
- Paatero, P., Tapper, U., 1994. Positive matrix factorization: a non-negative factor model with optimal utilization of error estimates of data values. *Environmetrics* 5, 111-126.
- Paatero, P., Hopke, P.K., Song, X.H., Ramadan, Z., 2002. Understanding and controlling rotations in factor analytic models. *Chemom. Intell. Lab. Syst.* 60, 253-264.
- Paatero, P., Eberly, S., Brown, S.G., Norris, G.A., 2014. Methods for estimating uncertainty in factor analytic solutions. *Atmos. Meas. Tech.* 7, 781-797.
- Pant, P., Harrison, R.M., 2013. Estimation of the contribution of road traffic emissions to particulate matter concentrations from field measurements: a review. *Atmos. Environ.* 77, 78-97.
- Pecorari, E., Squizzato, S., Ferrari, A., Cuzzolin, G., Rampazzo G., 2013a. WATERBUS: A model to estimate boats' emissions in "water cities". *Transport. Res. D-TR E*, 23, 73-80.
- Pecorari, E., Squizzato, S., Masiol, M., Radice, P., Pavoni, B., Rampazzo, G., 2013b. Using a photochemical model to assess the horizontal, vertical and time distribution of PM<sub>2.5</sub> in a complex area: Relationships between the regional and local sources and the meteorological conditions. *Sci. Total Environ.* 443, 681-691.
- Pecorari, E., Mantovani, A., Franceschini, C., Bassano, D., Palmeri, L., Grancazzo, G., 2015. Analysis of the effects of meteorology on aircraft exhaust dispersion and deposition using a Lagrangian particle model. *Sci Total Environ.* 541, 839-856.
- Petzold, A., Weingartner, E., Hasselbach, J., Lauer, P., Kurok, C., Fleischer, F., 2010. Physical properties, chemical composition, and cloud forming potential of particulate emissions from a marine diesel engine at various load conditions. *Environ. Sci. Technol.* 44, 3800-3805.
- R Core Team, 2015. R: A language and environment for statistical computing. R Foundation for Statistical Computing, Vienna, Austria. URL <http://www.R-project.org/>.
- Reche, C., Querol, X., Alastuey, A., Viana, M., Pey, J., Moreno, T., Rodriguez, S., Gonzalez, Y., Fernandez-Camacho, R., Sanchez de la Campa, A.M., de la Rosa, J., Dall'Osto, M., Prevot, A.S.H., Hueglin, C., Harrison, R.M. and Quincey, P., 2011. New considerations for pm, black carbon and particle number concentration for air quality monitoring across different European cities. *Atmos. Chem. Phys.* 11, 6207-6227.
- Reff, A., Eberly, S.I., Bhawe, P.V., 2007. Receptor modeling of ambient particulate matter data using positive matrix factorization: review of existing methods. *JAWMA* 57, 146-154.

- Rodríguez, S., Van Dingenen, R., Putaud, J.P., Martins-Dos Santos, S. Roselli, D., 2005. Nucleation and growth of new particles in the rural atmosphere of Northern Italy—relationship to air quality monitoring. *Atmos. Environ.* 39(36), 6734-6746.
- Salimi, F., Ristovski, Z., Mazaheri, M., Laiman, R., Crilley, L.R., He, C., Clifford, S., Morawska, L., 2014. Assessment and application of clustering techniques to atmospheric particle number size distribution for the purpose of source apportionment. *Atmos. Chem. Phys.* 14, 11883-11892.
- Seinfeld, J.H., Pandis, S.N., 2006. *Atmospheric Chemistry and Physics*, second ed.. In: *From Air Pollution to Climate Change* John Wiley & Sons, NewYork.
- Shi, J.P., Harrison, R.M., 1999. Investigation of ultrafine particle formation during diesel exhaust dilution. *Environ. Sci. Technol.* 33, 3730-3736.
- Squizzato, S., Masiol, M., Brunelli, A., Pistollato, S., Tarabotti, E., Rampazzo, G., Pavoni, B., 2013. Factors determining the formation of secondary inorganic aerosol: a case study in the Po Valley (Italy). *Atmos. Chem. Phys.* 13, 1927-1939.
- Squizzato, S., Masiol, M., 2015. Application of meteorology-based methods to determine local and external contributions to particulate matter pollution: A case study in Venice (Italy). *Atmos. Environ.* 119, 69-81.
- Stanier, C. O., Khlystov, A. Y. and Pandis, S. N., 2004. Nucleation Events During the Pittsburgh Air Quality Study: Description and Relation to Key Meteorological, Gas Phase, and Aerosol Parameters. *Aerosol Sci. Technol.* 38, 253-264.
- Stevens, R. G., Pierce, J. R., Brock, C. A., Reed, M. K., Crawford, J. H., Holloway, J. S., Ryerson, T. B., Huey, L. G., Nowak, J. B., 2012. Nucleation and growth of sulfate aerosol in coal-fired power plant plumes: sensitivity to background aerosol and meteorology. *Atmos. Chem. Phys.*, 12, 189-206.
- USEPA, 2014. EPA Positive Matrix Factorization (PMF) 5.0 - Fundamentals and user guide. EPA/600/R-14/108
- Valotto, G., Squizzato, S., Masiol, M., Zannoni, D., Visin, F., Rampazzo, G., 2014. Elemental characterization, sources and wind dependence of PM1 near Venice, Italy. *Atmos. Res.* 143, 371-379.
- Wang, X., Zhang, Y., Chen, H., Yang, X., Chen, J., Geng, F., 2009. Particulate nitrate formation in a highly polluted urban area: a case study by single-particle mass spectrometry in Shanghai. *Environ. Sci. Technol.* 43, 3061-3066.
- Wegner, T., Hussein, T., Hämeri, K., Vesala, T., Kulmala, M. Weber, S., 2012. Properties of aerosol signature size distributions in the urban environment as derived by cluster analysis. *Atmos. Environ.* 61, 350-360.
- Wormhoudt, J., Herndon, S.C., Yelvington, P.E., Lye-Miake, R.C., Wey, C., 2007. Nitrogen oxide (NO/NO<sub>2</sub>/HONO) emissions measurements in aircraft exhausts. *J. Propul. Power* 23, 906-911.
- Yue, W., Stölzel, M., Cyrys, J., Pitz, M., Heinrich, J., Kreyling, W.G., Wichmann, H.-E., Peters, A., Wang, S., Hopke, P.K., 2008. Source apportionment of ambient fine particle size distribution using positive matrix factorization in Erfurt, Germany. *Sci. Total Environ.* 398, 133-144.

Zhang, K.M., Wexler, A.S., Zhu, Y.F., Hinds, W.C., Sioutas, C., 2004. Evolution of particle number distribution near roadways. Part II: the 'Road-to-Ambient' process. *Atmos. Environ.* 38, 6655-6665.

Zhang, R., Khalizov, A., Wang, L., Hu, M., Xu, W., 2011. Nucleation and growth of nanoparticles in the atmosphere. *Chem. Rev.* 112, 1957-2011.

Zhou, L., Kim, E., Hopke, P.K., Stanier, C.O. Pandis, S., 2004. Advanced factor analysis on Pittsburgh particle size-distribution data special issue of aerosol science and technology on findings from the Fine Particulate Matter Supersites Program. *Aerosol Sci. Technol.* 38(S1), 118-132.

## TABLE LEGENDS

**Table 1.** Summary of PMF analysis.

**Table 2.** Spearman's correlations among extracted factors, common air pollutants and some micro-meteorological parameters. Only correlations significant at  $p < 0.001$  are shown;  $\rho > 0.6$  are bold faced  $0.35 < \rho < 0.6$  are in italic.

**Table 3.** Results of wind sector analysis for BC data. Data have been filtered by wind speeds  $> 1 \text{ m s}^{-1}$ .

## FIGURE LEGENDS

**Figure 1.** Map of the study area (left): some local sources are highlighted by different colours. Detailed view of the airport of Venice (right): the sampling site is shown as a star.

**Figure 2.** a) Boxplots of some analysed pollutants (line= median, box= inter-quartile range, whiskers=  $\pm 1.5 \times$  inter-quartile range). b) Diurnal variations of levels of measured pollutants computed over the hourly averaged data during the sampling period (e.g., 6:00 refer to averaged data between 6:00 and 7:00). Each plot reports the average level as a filled line and the associated 75th and 99th confidence intervals calculated by bootstrapping the data ( $n=200$ ). In purple particle number data from SMPS and APS, which were roughly categorised as: nucleation (14-30 nm), Aitken nuclei (30 to 100 nm), accumulation (0.1 to 1  $\mu\text{m}$ ) and coarse particles (1 to 20  $\mu\text{m}$ ); in red gaseous pollutants; in black non-gaseous pollutants and in green some micro-meteorological variables. Data of airport traffic only refer to civil aviation movements.

**Figure 3.** Polar plots of analysed air pollutants. The position of the wind speed scale on each plot corresponds to the location of the runway. PNC and BC data were hourly-averaged to be matched with wind data.

**Figure 4.** Distributions particle number and volume categorised by daytime (01:00-07:00; 07:00-13:00; 13:00-19:00; 19:00-01:00 local time). Lines represent the median concentrations, while shaded areas report the 25th-75th percentile intervals.

**Figure 5.** Results of cluster analysis. Average cluster PNSD spectra (left) are reported as solid red lines along with: (i) their 10th, 25th, 75th and 90th percentile spectrum as shaded areas; (ii) the volume size distributions (dashed blue line); (iii) the hourly counts and (iv) the wind roses associated to each cluster.

**Figure 6.** Selected period (23th to 27th May). The plots represent (from upper to the bottom): (1) hourly counts of number of clusters; (2) airport traffic (arrivals+departures); (3) solar irradiation; (4) nitrogen oxide concentration; (5) sulphur dioxide concentration; (6) particle number concentration for the nucleation range (14-30 nm); (7) particle number concentration for the Aitken range (30-100 nm); (8) particle number concentration for the accumulation range (100-1000 nm); (9) BC concentration; (10) contour plots of SMPS data.



- Figure 7.** Number (black solid line) and volume (red dashed line) distributions for the six factors extracted by the PMF model. Data are expressed as normalised fractions on the total from the final solution (FPEAK=2.5).
- Figure 8.** Diurnal variations, polar plot and polar annulus of the six factors extracted from the PMF model. Diurnal variations report the average level as a filled line and the associated 75th and 99th confidence intervals calculated by bootstrapping the data (n=200).
- Figure 9.** Some CCFs computed among PMF factor contributions and other pollutants.
- Figure 10.** a) Polarplot of BC (hourly averaged data) during the whole sampling campaign; b) boxplots of the BC levels on filtered data for wind sectors and  $ws > 1 \text{ m s}^{-1}$  pollutants (line= median, box= inter-quartile range, whiskers=  $\pm 1.5 \times$  inter-quartile range).

**Table 1.** Summary of PMF analysis.

No.	Most probable source	Main modes		Contributions		Peak hours (local time)	Significant correlations at $p<0.001$ , $\rho>0.35$ <i>positive (negative)</i>
		Dominant PNSD	PVSD	PNSD % (95th confidence interval)	PVSD %		
1	<b>Nucleation</b>	15-20 nm	200 nm; 2 $\mu$ m	43.8 (43.4-44.1)	1.1	12am-1pm	NO, OX, solar irr., air temp.
2	<b>Traffic</b>	35-40 nm	80-90; 500 nm	25.5 (25.3-25.9)	4.8	6am-8am; 9pm-11pm	NO <sub>2</sub> , NO <sub>x</sub> , BC, (O <sub>3</sub> )
3	<b>Airport</b>	<14nm; 80 nm	200; 500 nm, 5 $\mu$ m	20.3 (20.1-20.5)	19.6	—	—
4	<b>Nighttime nitrate</b>	30 nm; 200 nm	400 nm; 2.5 $\mu$ m	5.9 (5.8-6.1)	41.2	5am-7am	NO <sub>2</sub> , BC, PM <sub>2.5</sub> , (O <sub>3</sub> ), (OX), (SO <sub>2</sub> ), (wind speed)
5	<b>Regional pollution</b>	60 nm	2-3 $\mu$ m	3 (2.4-3.1)	21.1	12pm-6am	CO, PM <sub>2.5</sub>
6	<b>Local resuspension</b>	25 nm	5 $\mu$ m	1.5 (1.3-1.6)	12.2	4am-6am	(O <sub>3</sub> ), (OX), (solar irr.), (air temp.), (wind speed)



**Table 2.** Spearman's correlations among extracted factors, common air pollutants and some micro-meteorological parameters. Only correlations significant at  $p < 0.001$  are shown;  $\rho > 0.6$  are bold faced  $0.35 < \rho < 0.6$  are in italic.

Factors	CO	NO	NO <sub>2</sub>	NO <sub>x</sub>	O <sub>3</sub>	OX	SO <sub>2</sub>	BC	PM <sub>2.5</sub>	Wind speed	Air temp.	Solar irr.
<b>Factor 1: Nucleation</b>		<i>0.37</i>			<i>0.31</i>	<i>0.41</i>	<i>0.33</i>			<i>0.20</i>	<i>0.52</i>	<i>0.47</i>
<b>Factor 2: Traffic</b>	<i>0.25</i>		<i>0.44</i>	<i>0.41</i>	<i>-0.43</i>	<i>-0.31</i>	<i>-0.23</i>	<i>0.41</i>	<i>0.19</i>	<i>-0.23</i>	<i>-0.22</i>	
<b>Factor 3: Airport</b>	<i>0.31</i>	<i>0.19</i>						<i>0.20</i>				
<b>Factor 4: Nighttime nitrate</b>	<i>0.31</i>		<i>0.37</i>	<i>0.33</i>	<i>-0.53</i>	<i>-0.47</i>	<i>-0.43</i>	<b>0.64</b>	<i>0.48</i>	<i>-0.54</i>	<i>-0.30</i>	<i>-0.17</i>
<b>Factor 5: Regional pollution</b>	<i>0.52</i>				<i>-0.30</i>	<i>-0.31</i>	<i>-0.39</i>	<i>0.29</i>	<i>0.41</i>	<i>-0.23</i>	<i>-0.33</i>	<i>-0.25</i>
<b>Factor 6: Local resuspension</b>			<i>0.24</i>	<i>0.20</i>	<i>-0.55</i>	<i>-0.50</i>	<i>-0.35</i>	<i>0.30</i>	<i>0.33</i>	<i>-0.45</i>	<i>-0.54</i>	<i>-0.47</i>

1393 **Table 3.** Results of wind sector analysis for BC data. Data have been filtered by wind speeds  $>1 \text{ m s}^{-1}$ .

1394

Location	Sector <i>degree</i>	Mean $\pm$ St.Dev. $\mu\text{g m}^{-3}$	Median (25th-75th percentile) $\mu\text{g m}^{-3}$
Urban area of Mestre	240–280	1.0 $\pm$ 0.4	1 (0.8–1.2)
Porto Marghera	210–240	0.7 $\pm$ 0.3	0.7 (0.4–0.8)
Venice	170–210	0.8 $\pm$ 0.3	0.8 (0.7–1)
Island of Murano	150–170	0.8 $\pm$ 0.4	0.6 (0.6–0.9)
VCE airfield	30–150	0.7 $\pm$ 0.4	0.7 (0.5–0.9)
Other directions	280–30	1.5 $\pm$ 0.8	1.4 (0.9–1.9)

1395

1396

1397

1398

1399

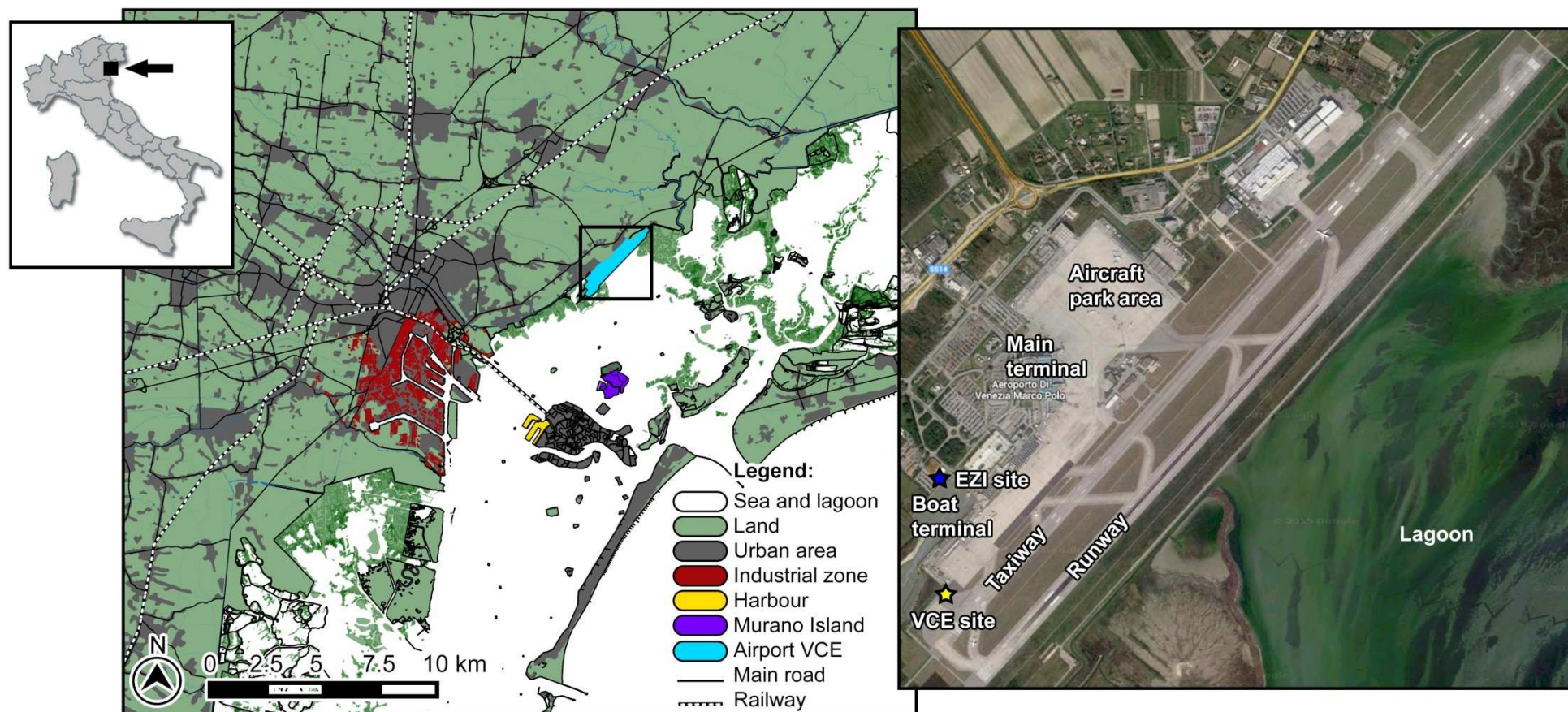


**Figure 1.** Map of the study area (left): some local sources are highlighted by different colours. Detailed view of the airport of Venice (right): the sampling site is shown as a star.

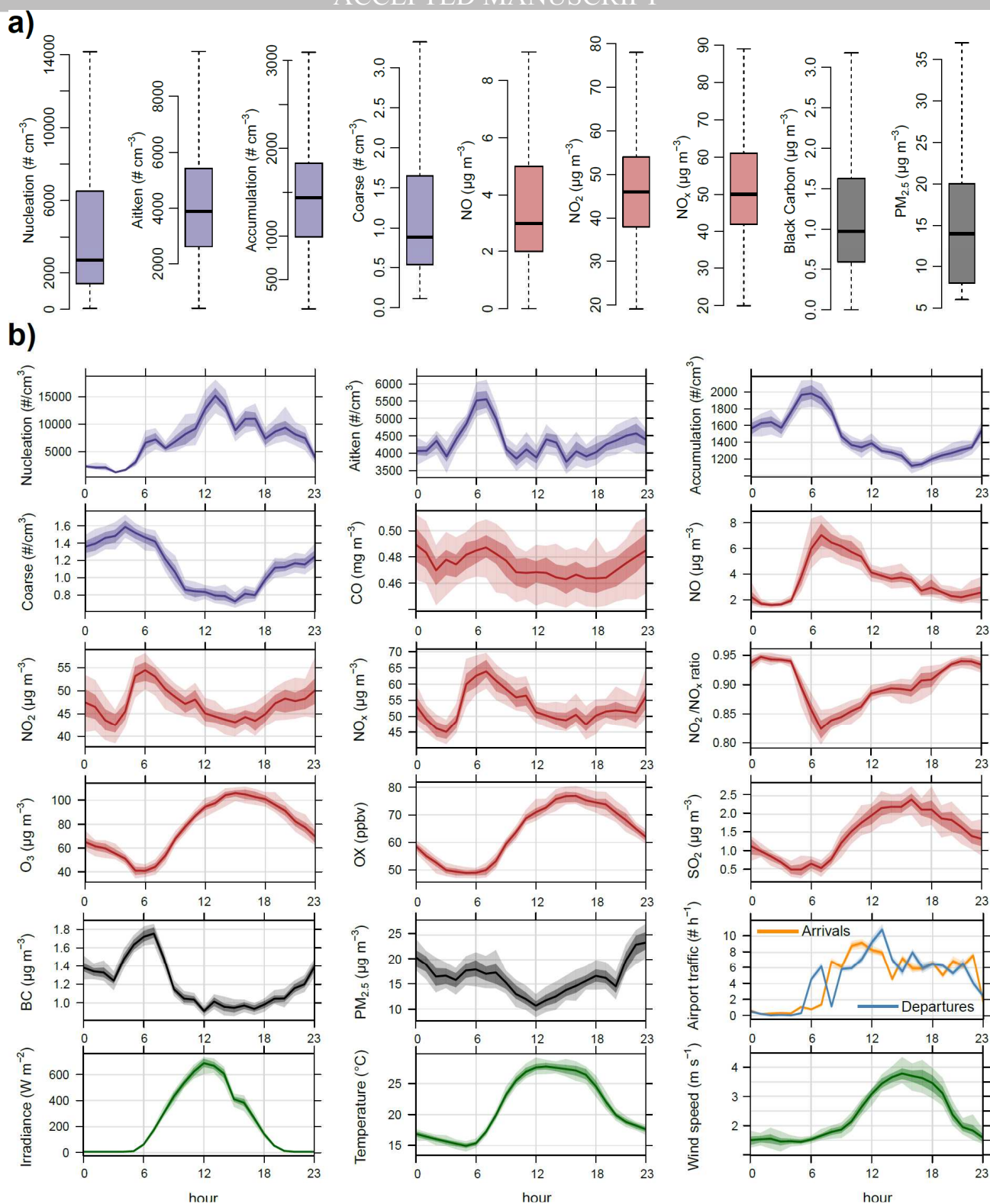


**Figure 2.** a) Boxplots of some analysed pollutants (line= median, box= inter-quartile range, whiskers=  $\pm 1.5 \times$  inter-quartile range). b) Diurnal variations of levels of measured pollutants computed over the hourly averaged data during the sampling period (e.g., 6:00 refer to averaged data between 6:00 and 7:00). Each plot reports the average level as a filled line and the associated 75th and 99th confidence intervals calculated by bootstrapping the data ( $n=200$ ). In purple particle number data from SMPS and APS, which were roughly categorised as: nucleation (14–30 nm), Aitken nuclei (30 to 100 nm), accumulation (0.1 to 1  $\mu\text{m}$ ) and coarse particles (1 to 20  $\mu\text{m}$ ); in red gaseous pollutants; in black non-gaseous pollutants and in green some micro-meteorological variables. Data of airport traffic only refer to civil aviation movements.



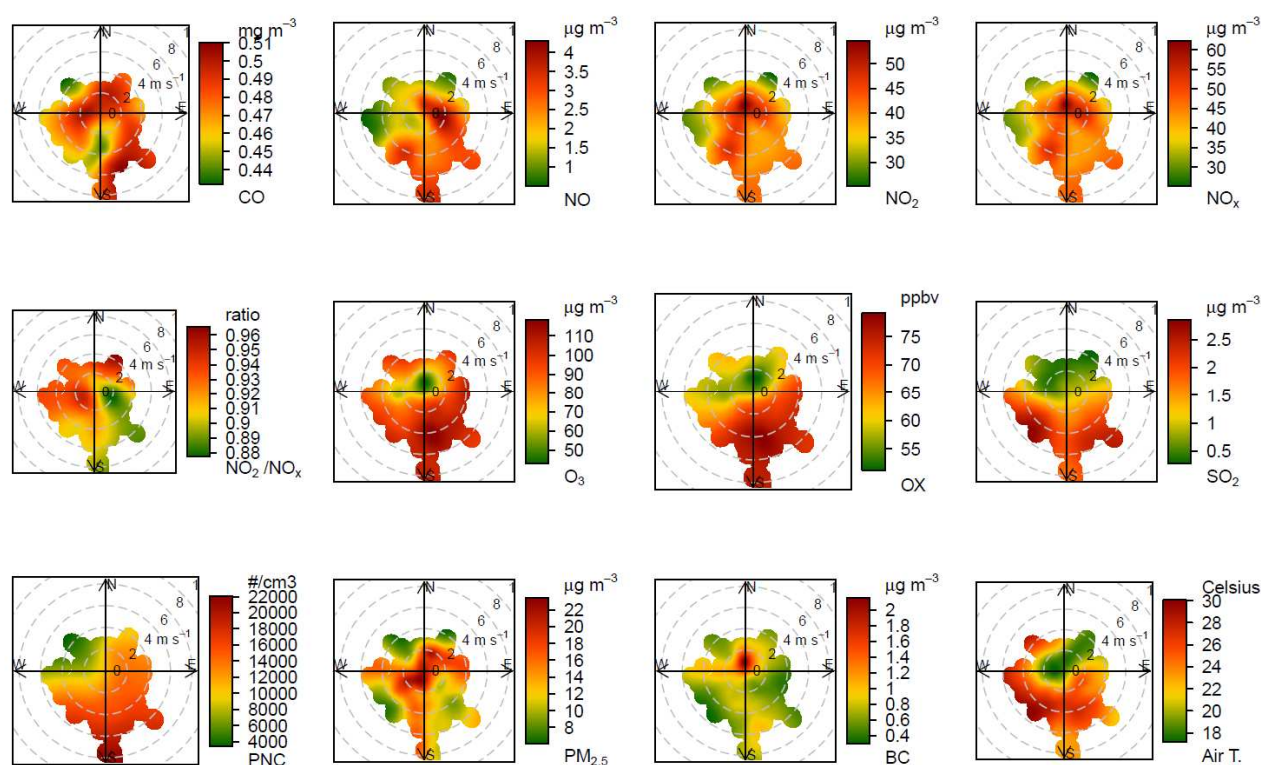


**Figure 3.** Polar plots of analysed air pollutants. The position of the wind speed scale on each plot corresponds to the location of the runway. PNC and BC data were hourly-averaged to be matched with wind data.

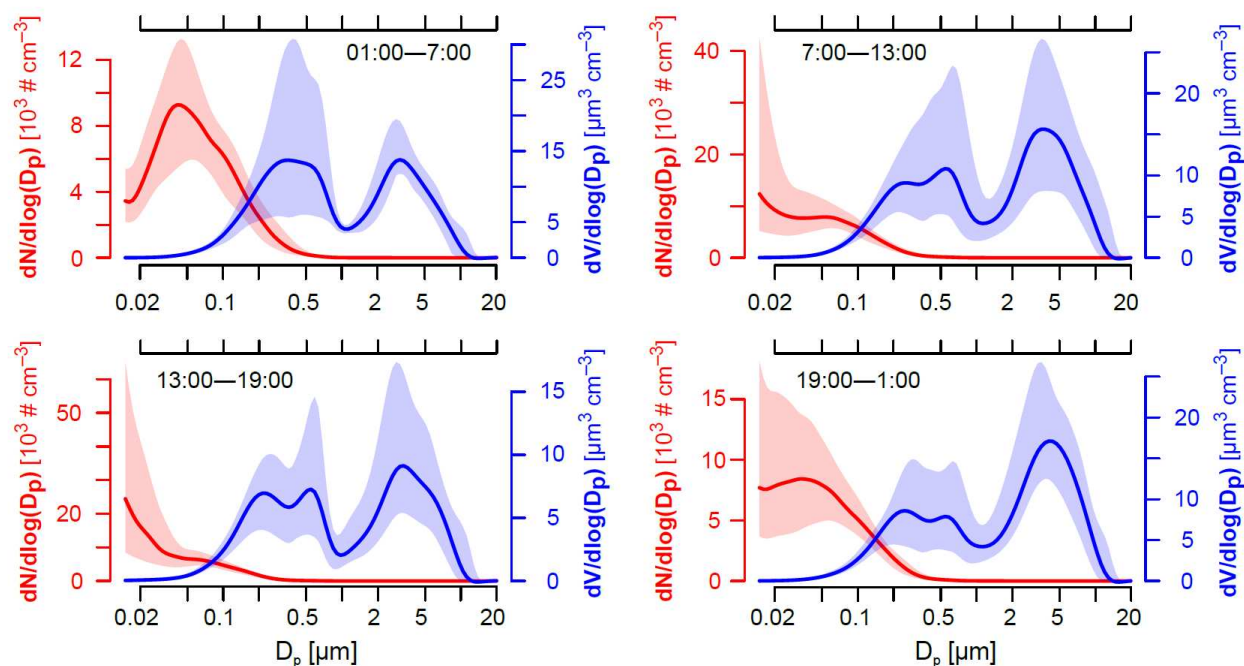


**Figure 4.** Distributions particle number and volume categorised by daytime (01:00-07:00; 07:00-13:00; 13:00-19:00; 19:00-01:00 local time). Lines represent the median concentrations, while shaded areas report the 25th-75th percentile intervals.

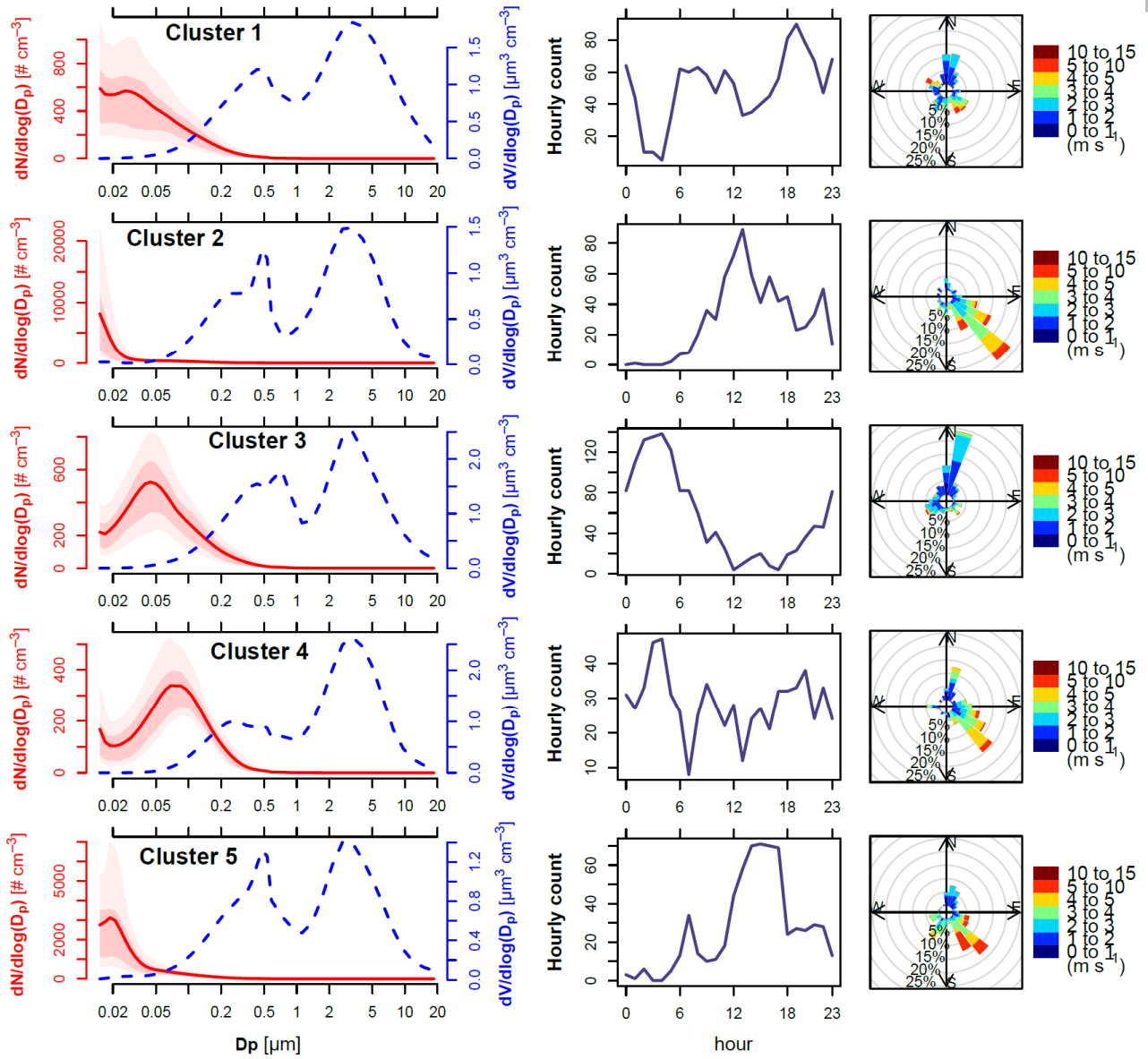


**Figure 5.** Results of cluster analysis. Average cluster PNSD spectra (left) are reported as solid red lines along with: (i) their 10th, 25th, 75th and 90th percentile spectrum as shaded areas; (ii) the volume size distributions (dashed blue line); (iii) the hourly counts and (iv) the wind roses associated to each cluster.



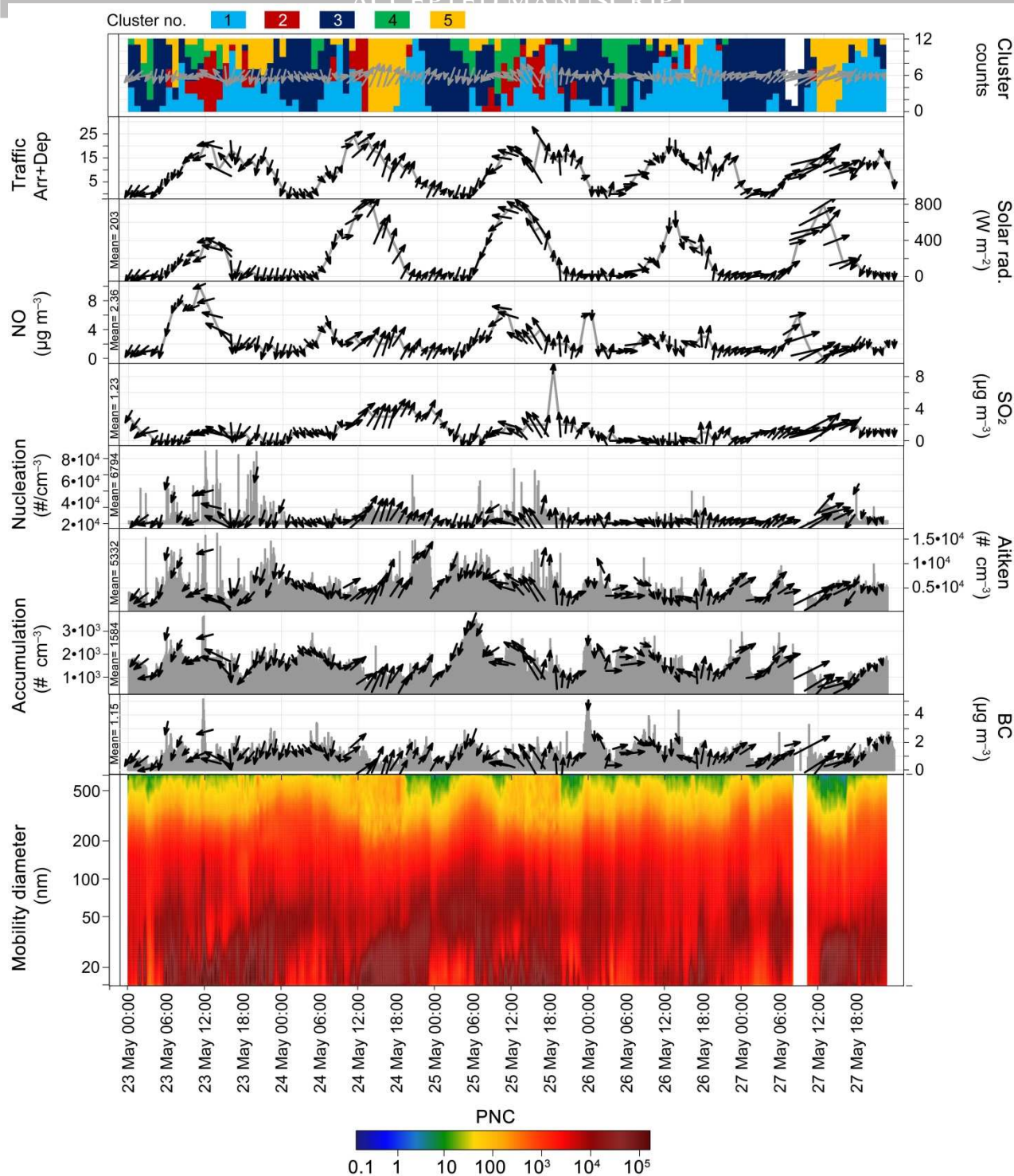


**Figure 6.** Selected period (23th to 27th May). The plots represent (from upper to the bottom): (1) hourly counts of number of clusters; (2) airport traffic (arrivals+departures); (3) solar irradiation; (4) nitrogen oxide concentration; (5) sulphur dioxide concentration; (6) particle number concentration for the nucleation range (14-30 nm); (7) particle number concentration for the Aitken range (30-100 nm); (8) particle number concentration for the accumulation range (100-1000 nm); (9) BC concentration; (10) contour plots of SMPS data.

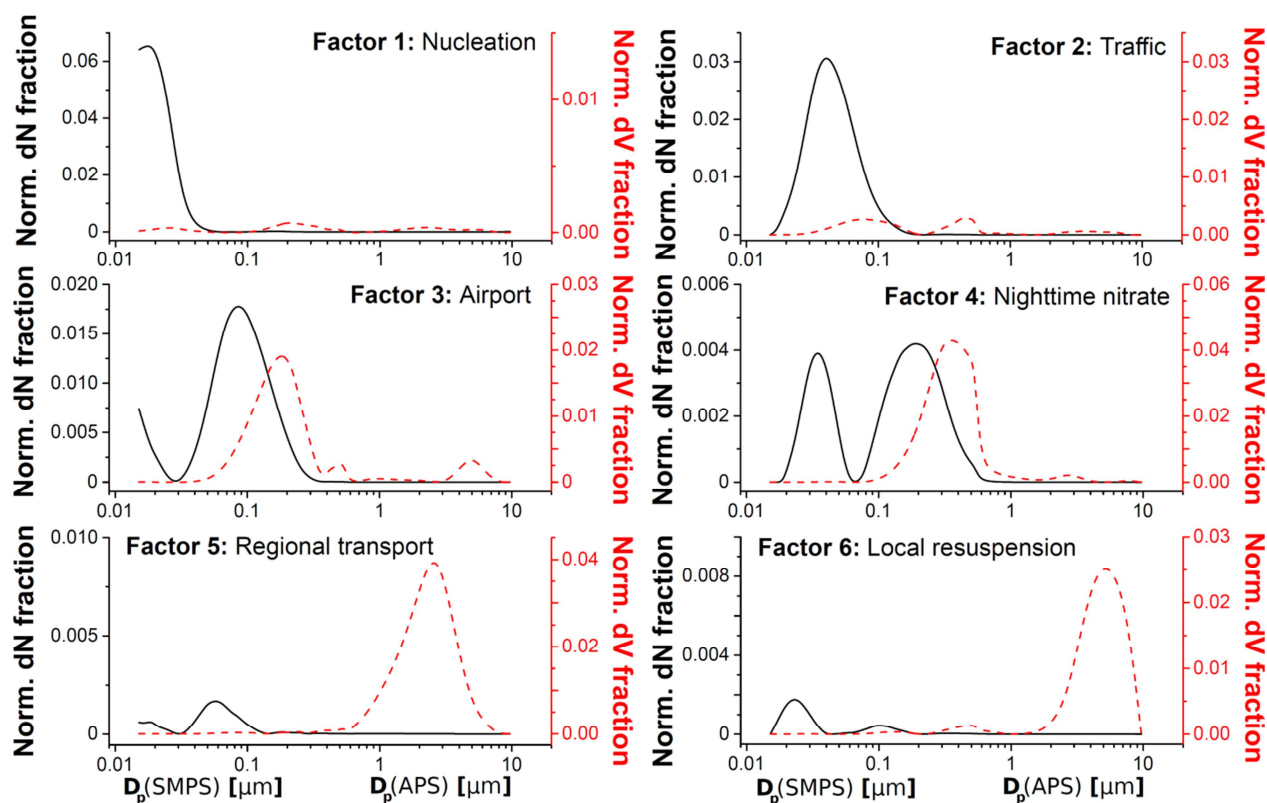
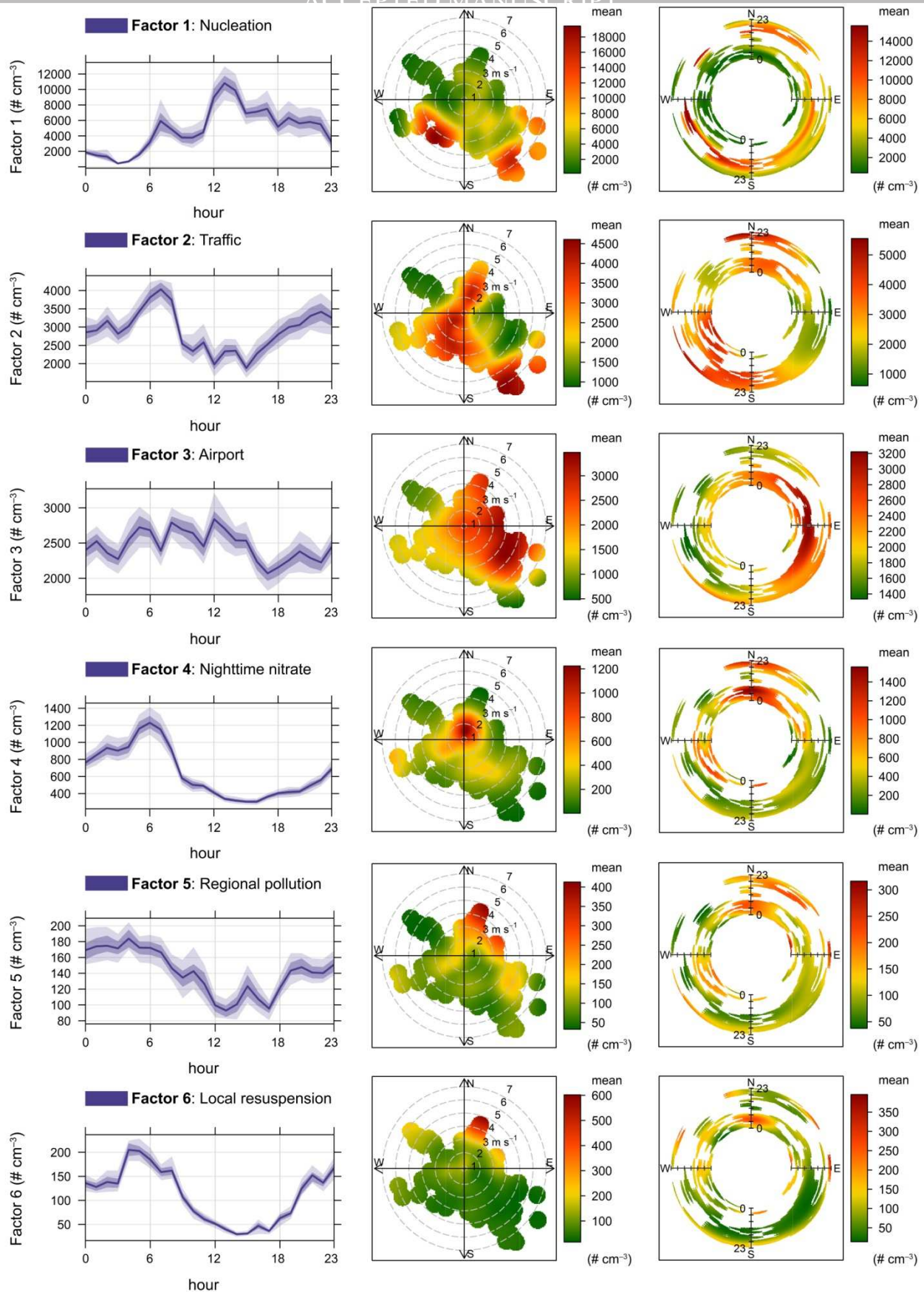


**Figure 7.** Number (black solid line) and volume (red dashed line) distributions for the six factors extracted by the PMF model. Data are expressed as normalised fractions on the total from the final solution (FPEAK=2.5).



1448

1449

1450

1451

**Figure 8.** Diurnal variations, polar plot and polar annulus of the six factors extracted from the PMF model. Diurnal variations report the average level as a filled line and the associated 75th and 99th confidence intervals calculated by bootstrapping the data (n=200).

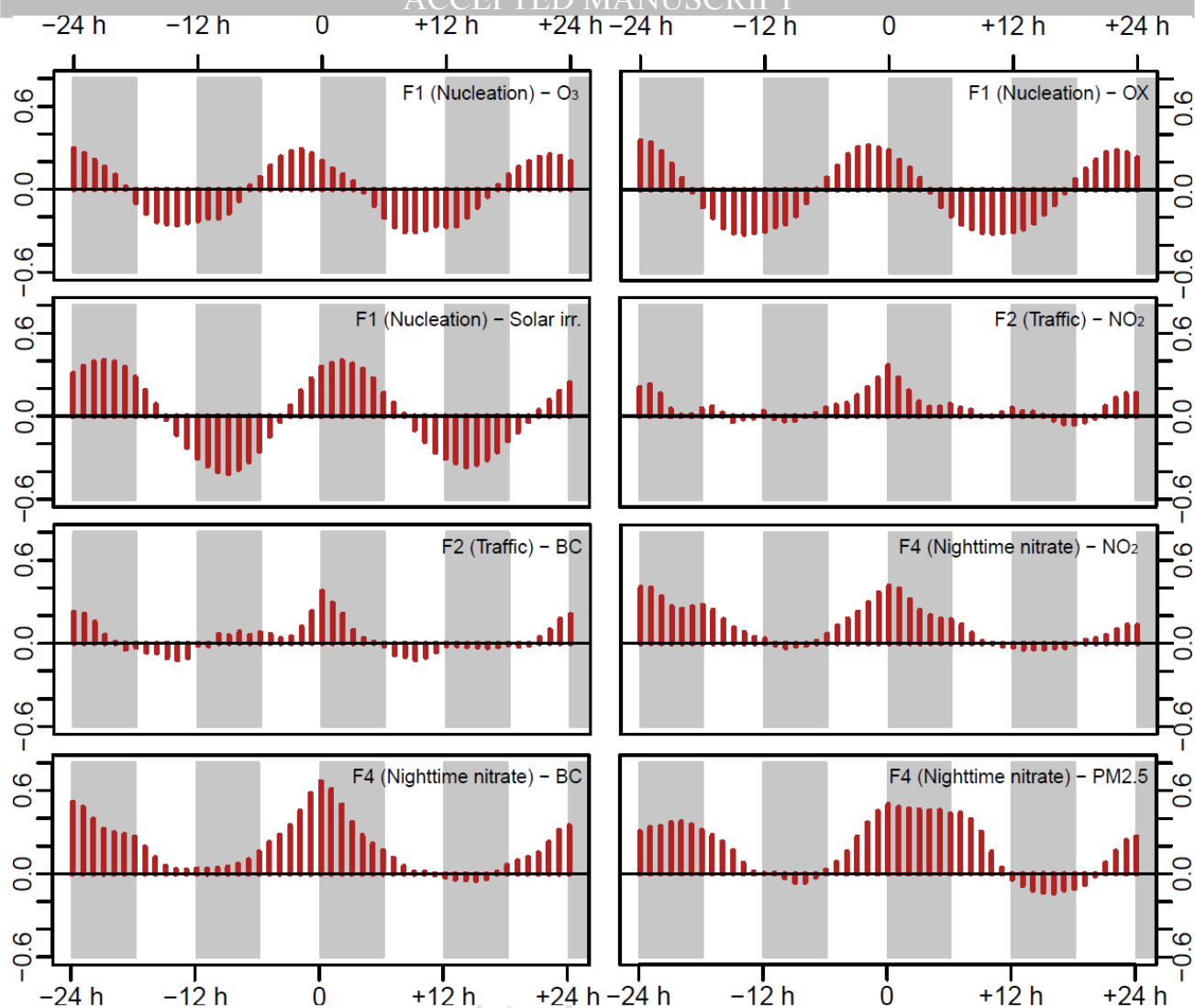


**Figure 9.** Some CCFs computed among PMF factor contributions and other pollutants.



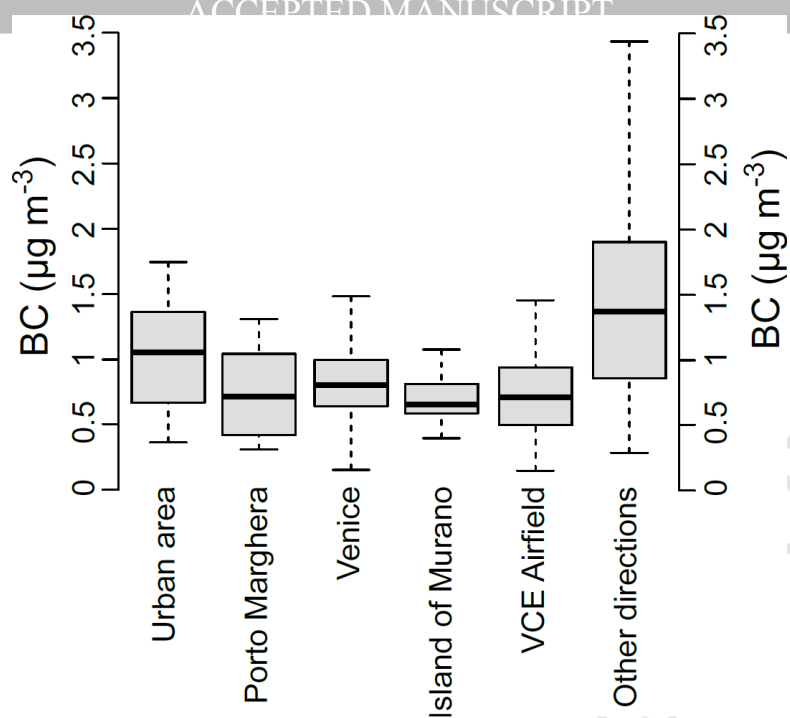


**Figure 10.** a) Polarplot of BC (hourly averaged data) during the whole sampling campaign; b) boxplots of the BC levels on filtered data for wind sectors and  $ws > 1 \text{ m s}^{-1}$  pollutants (line= median, box= inter-quartile range, whiskers=  $\pm 1.5$ \*inter-quartile range).